PB97-105209

Final Performance Report

EVALUATION OF RESPIRATOR FILTERS FOR ASBESTOS FIBERS

Submitted to the National Institute of Safety and Health
Grant No. 5R01 OH02922-02
Project Director: Dr. Roy M. Fleming

Principal Investigator: Yung Sung Cheng

Co-Investigators: Bijian Fan, Thomas D. Holmes, and Hsu Chi Yeh

Inhalation Toxicology Research Institute
Albuquerque, New Mexico 87185
January 27, 1996

REPRODUCED BY: NTIS
U.S. Department of Commerce
National Technical Information Service
Springfield, Virginia 22161

TABLE OF CONTENTS

LIST OF ABBREVIATIONS

DOS	Di-octyl sebacate
EM	Electron microscope
EPA	Environmental Protection Agency
FAM	Fiber aerosol monitor
NIOSH	National Institute of Occupational Safety and Health
OSHA	Occupational Safety and Health Agency
PEL	Permissible exposure limit
QCM	Quartz crystal microbalance
RAM	Real-time aerosol monitor
SSPD	Small-scale powder disperser

LIST OF FIGURES

LIST OF TABLES

SIGNIFICANT FINDINGS

(1) Only high-efficiency filters performed consistently on both the spherical test aerosols and three types of asbestos fibers. The high-efficiency filters tested were >99% efficient in all cases. Neither the surface charge potential of filter cartridges nor the charge status of fibers appeared to affect filter performance. On the other hand, the performance of low-efficiency filters and masks deteriorated when the charge potential on the filter was removed or fiber aerosols were discharged.

(2) The surface charge measurements of the respirator filters showed that some filters, including those used in disposable respirators, are charged to enhance the collection efficiency. Our data also showed that surface charges were decreased in a high-temperature, high-humidity environment and disappeared after 1 week. While deposition of spherical particles and fibers in the charged disposable filter was enhanced, the collection efficiency of filter cartridges that did not carry electrostatic charges was not. Similar effects were found for the charge status on fibers. The aerosols in equilibrium charge status were found to have lower deposition efficiency than the charged aerosols. Because many aerosols found in the work environment are aged and in the charge equilibrium, our results imply that they would not be removed as efficiently.

(3) Shorter fibers had a higher penetration rate, which indicates that fiber interception is an important deposition mechanism. Experimental penetration data were mapped using contours of equal penetration in a two-dimensional plot. The observed data showed one region of maximum penetration for each condition. The mathematical model provides a similar penetration contour. The maximum penetration occurred at the region of fiber diameter and length where the interception and diffusion deposition are at a minimum.

(4) Because of the filtration of longer fibers, the biological effects of shorter fibers that are inhaled may be different from bulk fiber aerosols. These differences may be related to deposition pattern, deposition efficiency, clearance, and biological activities of inhaled fibers.

(5) Fibers can penetrate leaks in the face mask seal, with increased penetration for larger leaks. The fibers that penetrated had similar size distributions as the bulk aerosols. Therefore, for respirators with high-efficiency filters, penetration through face mask leaks can be a serious problem for respiratory protection of workers.

USEFULNESS OF FINDINGS

Our findings confirm the current OSHA guidelines, which state that only high- efficiency filters should be used for respiratory protection of workers dealing with asbestos and other types of fibers. However, we have found that a significant fraction of fibers can still penetrate through leaks in the face seal and other parts of the respirator. It is therefore important to ensure a proper fit before a worker wears the respirator. The current procedures for testing the fit of a respirator use spherical or ambient aerosols. Whether this procedure is adequate for fiber aerosols is not known and should be studied.

We have also found that some filter cartridges had substantial charge potential, which enhance filter performance. However, the surface charge may disappear quickly in high- temperature, high-humidity environments, and the performance of the filter may deteriorate significantly. There are many implications in this finding. For example, NIOSH test procedures may require a different way to condition filter cartridges prior to an aerosol challenge. The test aerosol should also be charge neutralized. It may also be necessary to find ways to extend the shelf life of charged filter cartridges or masks.

ABSTRACT

Current OSHA guidelines require the use of respirators fitted with high-efficiency filters to protect workers in environments where they are at risk of exposure to asbestos and manmade fibers. These filters must be approved under NIOSH certification criteria based on penetration tests using spherical aerosols. Fiber aerosols are known to have different aerodynamic behaviors than spherical particles and usually carry higher electrostatic charges. Because the carcinogenicity of asbestos and other fibers are known to be due, in part, to fiber dimensions, it is very important to know the efficiency of the respirator filters in relation to fiber dimension. We have investigated the effects of fiber dimensions, flow rate, and charge status of filter cartridges on the penetration of fiber aerosols. Four types of test respirator filters including two for passive respirators, one for a powered respirator, and one disposable respirator were selected. Surface charges on respirator filters have been determined using a non-contact field electrostatic field meter. Penetration tests were performed for filter cartridges before and after charge neutralization. The surface charge measurements on the respirator filters showed that some filters including those used in disposable respirators are charged to enhance the collection efficiency. Only high-efficiency filters performed consistently for both spherical test aerosols and the three types of asbestos fibers. The surface charge potential of filter cartridges and charge status of fibers did not appear to affect the performance of these filters. On the other hand, the performance of low-efficiency filters and masks had deteriorated for aerosols when the charge potential on the filter was removed and/or fiber aerosols discharged. Our data also showed that the surface charges decreased in a high-temperature, high-humidity environment and disappeared after 1 week. Deposition of spherical particles and fibers in the charged disposable filter was enhanced. On the other hand, for filter cartridges that did not carry electrostatic charges, collection efficiency was not enhanced. Shorter fibers had higher penetration rates, which indicates that fiber interception is an important deposition mechanism. Our data showed one region of maximum penetration for each condition. The mathematical model provides a similar penetration contour. The maximum penetration occurred in the region of fiber diameter and length where the interception and diffusion deposition are at a minimum. The fibers could penetrate the face mask seal, with increased penetration for larger leaks. The fibers that penetrated had similar size distributions as the bulk aerosols. This factor will be a major concern for respiratory protection against fiber aerosols.

BODY OF REPORT
BACKGROUND

Exposure by inhalation to asbestos fibers may lead to primary lung cancers, mesothelioma, and pulmonary and pleural fibrosis. The carcinogenicity potential of asbestos fibers has been shown to correlate with fiber dimensions and their durability in the lung (Stanton and Wrench, 1972; Pott *et al.*, 1983). Concerns about the health risks associated with exposure to asbestos fibers have resulted in restricting their use in many applications, including thermal insulation and construction materials. However, many public buildings and private houses that contained asbestos as building or insulation material now require removal of the asbestos, and the asbestos abatement industry continues to grow. Manmade fibrous material, such as fiberglass and ceramic fibers, have been developed to replace asbestos. Silicon carbide, silicon nitride, and other fibers are important constituents of composite materials that have applications in aerospace and automotive industries. Health effects of inhalation exposures to these manmade fibers have been evaluated (Drew *et al.*, 1988; Smith *et al.*, 1987). Potential sources of exposure to fibrous materials in occupational environments will continue to increase with expansion of commercial applications.

OSHA and EPA have set the permissible exposure limit (PEL) for asbestos fibers at 0.2 fibers mL^{-1} of air in occupational environments (EPA, 1986; OSHA, 1986). Engineering control and work practice are the preferred methods to reduce worker exposure in these environments. However, if these methods cannot reduce the asbestos concentration below the PEL, then respiratory protection is required to minimize exposure. The OSHA guidelines also require respiratory protection during maintenance and repair activities and in emergencies.

Fiber particles with elongated shapes (ratio of length to diameter > 3:1) have different aerodynamic characteristics than spherical particles of the same volume and density. The aerodynamic behavior of fibrous aerosols is largely dependent on the diameter of the fiber. with the length of the fiber having a minor influence (Stöber, 1973; Cheng, 1986). Asbestos fibers found in most occupational environments have wide size distributions in both diameter and length (Walton, 1982). The diameter of respirable asbestos fibers ranges from 0.01 to 3.0 μm, and the length ranges from 0.1 to 60 μm (Walton, 1982). Manmade fibers, such as glass, ceramic, and carbon fibers, have a diameter between 0.1 to 10 μm and an aspect ratio ranging from 3 to 60. Because of the wide size range of fiber aerosols, it is essential that a respirator certified for use on one type of fiber is also suitable for other types of fiber aerosols with potentially very different size characteristics.

Data are limited on fiber filtration through respirator filters. Weeks and Burns (1970) reported 0 to 2.6% penetration of a chrysotile asbestos aerosol through eight different respirator filters. Brosseau *et al.* (1990) reported 0.001 to 0.2% penetration of an amosite aerosol at 32 L min^{-1} constant flow. They also tested the same filters with silica aerosols. Ortiz *et al.* (1988) compared the penetration of chrysotile asbestos and an oil test aerosol of di(2-ethylhexyl) sebacate (DEHS)

through filter cartridges approved by NIOSH (1987;1990). A lower penetration rate (0 to 3%) was observed for asbestos than for DEHS aerosols (0 to 30%), when the filters were taken from the package without extended storage time. However, after a 1-week storage at a high temperature (38°C) and in high humidity (99%+), the fiber penetration increased to 20% for some filters. Similar deterioration of filter performance was found after filters received a substantial particle load of DEHS or were instilled with water mist. This level of fiber penetration (20%) could certainly result in workers being exposed to fiber concentrations that exceed the PEL in work environments with > 20 fibers mL^{-1} concentration, even if they wore respirators. The only filter that performed consistently under all conditions was a high-efficiency filter. Because OSHA has particular concerns about the inconsistency in the reported observations of fiber aerosols through medium- (> 99%) and low- (> 95%) efficiency filters, only high-efficiency filters (> 99.97%) can be used when air-purifying respirators are needed for worker protection against asbestos fibers. (NIOSH, 1987; 1990).

Because earlier studies were not designed to evaluate the filtration processes for fibers, there are no data on the effects of particle size and flow rate on filtration efficiency. Only the overall penetration, which is the average penetration of a fiber with wide length and diameter distributions, has been reported; size distributions of fiber aerosols that penetrate a filter and enter the respiratory system have not been determined. This is an important concern in the respiratory protection of workers, because of the importance of fiber dimensions to the carcinogenicity of asbestos (Stanton and Wrench, 1972; Pott *et al.*, 1983). On the other hand, electrostatic charges associated with filter cartridges have been implicated in the inconsistent results of filter performance reported by Ortiz *et al.* (1988), but their experimental design did not provide sufficient information to test this hypothesis. No attempts were made to determine the electrostatic charges of fibers, nor the electrical potential of filter cartridges under test conditions.

SPECIFIC AIMS

The specific aims of this research were to quantify the performance of respirator filters used to protect workers in environments where they may be at risk of exposure to asbestos and manmade fibers, and to elucidate the mechanical and electrical deposition mechanisms for the filtration of fiber aerosols. This information will help to determine which types of fiber aerosols are most likely to penetrate the respirable filters and to predict the performance of respirator filters under different field conditions.

Specific Aim 1: Filter penetration tests using three different asbestos fibers will yield useful information on the effect of fiber dimension. Electrostatic charges on fiber aerosols and filter cartridges will be neutralized, and only mechanical deposition processes of fiber filtration, such as diffusion, impaction, and interception, will be investigated. Two flow rates will be investigated. Dimensions of fibers that are most likely to penetrate a respirator filter will be ascertained.

Specific Aim 2: Penetration tests will also be performed using the spherical di-octyl sebacate (DOS) aerosol according to the NIOSH test procedures. A direct comparison of the filter performance between the fiber aerosols and spherical aerosols will be made.

Specific Aim 3: Freshly generated asbestos fibers usually carry high electrostatic charges. These fibers will be neutralized to the Boltzmann charge equilibrium. Some filter cartridges consisting of materials of low conductivity may carry electrostatic charges; these charges may be lost during storage under conditions of high temperature and high humidity. Fiber penetration through filters fresh from the package and stored under these conditions will be studied. Filtration under four experimental conditions will be tested by combining the charge status of fiber aerosols and filter cartridges.

Specific Aim 4: Filtration of fiber aerosols in a fan model filter using stainless steel wire screens will be investigated. Charge-neutralized asbestos fiber aerosols will be used. The fiber filtration model will be established by modifying the existing model, and this model will be further extended to predict fiber aerosol collection on respirator filters.

Specific Aim 5: Penetration of fiber aerosols through leaks in the face seal will be measured in a half-face respirator mounted on a simulated face. These leaks will be created by placing wires of 1.0 and 2.0 mm diameter in the respirator. Three asbestos fibers will be used for the test.

PROCEDURES AND METHODOLOGY

Test Respirator Filters

Characterization of Test Filters

Four types of respirator filters were used in the study: 1) a high-efficiency filter, AOR57A (American Optical Corp., Southbridge, MA), 2) a dust/fume/mist filter cartridge, (Type S, MSA, Pittsburgh, PA, 3) a high-efficiency filter for powered respirators (Type A, MSA, Pittsburgh, PA), and 4) a disposable, low-efficiency filter (3M8710, 3M, St. Paul, MN). Following current NIOSH test procedures, the AOR57A and dust/fume/mist filters, which are used in dual cartridges, were tested at 16 and 42.5 L min^{-1}; the disposable-type filter and the filter for the powered respirators were tested at 32 and 85 L min^{-1}. Physical properties of the test filters that may have influenced the aerosol penetration were measured, including fiber diameter, total filtration area, filter thickness, filter solid fraction, and filter charges.

The fiber diameter was determined by examining the filter in an Olympus microscope (Scientific Instr. Co., Phoenix, AZ) coupled with an TV monitor and a desktop computer. An image analysis software (Optimus 5.0, Optimus Corp., Seattle, WA) was used to determine the fiber diameter. The filter solid fraction was determined by measuring the filter thickness and filter volume occupied by filter material. The volume of the filter sample was measured using a helium pycnometer (Multipycnometer, Quantachrome Corp., Syossett, NY). The surface charge measurements are described in the following section.

The measured physical properties of the four respirator filters are listed in Table 1. These values were used in the mathematical model to calculate theoretical prediction of filter performance.

Filter Surface Charge Measurements

The hypothesis postulated was that an increased electrical charge on a filter cartridge would increase the efficiency of the filter. To test this hypothesis, filter cartridges were used directly from the box and after treatment with an antistatic fluid (Zero Charge, Tech Spray, Amarillo, TX). The surface charge on the filters before and after the treatment was measured with an electrostatic field meter (Model 245, Monroe Electronics, Lyndonville, NY). The field was carefully placed on a movable table with a nonconducting surface (Daedal Inc., Harrision City, PA). The probe of the field meter was placed about 5 cm from the surface to measure the electrical field and the surface charge. Measured values of nine equally spaced locations on the filter surface were obtained and the mean value determined.

Respirators are not as efficient under high-temperature, high-humidity conditions (Ortiz *et*

al., 1988). However, the mechanism triggering the decreased performance has not been elucidated. We hypothesized that this deficiency was related to the electrostatic charge status of the filter. To test this, we placed new filter cartridges in a oven (Model 5851, National Appliance Co., Portland, OR) maintained at 38°C and >90% relative humidity for up to 11 days. The filters were taken out from time to time for surface charge measurement.

Test Materials

Three asbestos fibers of different diameters were tested: an ultrafine chrysotile (Calidria), a special asbestos; a UICC crocidolite with a mean diameter of 0.08-0.1 μm; and a UICC amosite (Davis *et al.*, 1986; Gentry *et al.*, 1989). The diameters of these fibers ranged from 0.02 to 1.4 μm where the dominant deposition mechanism in the filtration process changes from diffusional deposition to inertial deposition. We expected to find the maximum penetration size by using these fibers in the filtration study. The wide range of fiber lengths (0.2 to 10 μm) was also important to examine as a direct interception mechanism.

Penetration tests with the same respirator filters were performed using the DOS (Sigma Chemical Co., St. Louis, MO) aerosol according to NIOSH test procedures. The overall penetration was estimated by measuring upstream and downstream concentrations. A direct comparison of the filter performance between the fiber aerosols and the spherically shaped DOS aerosols was obtained.

Experimental Apparatus

Spherical Particle Penetration of the Filters

The experimental setup for measuring fractional penetration of DOS aerosols in the test respirator filters is shown schematically in Figure 1. A TSI condensation aerosol generator (model 3076, St. Paul, MN) was used (Liu and Lee, 1975). DOS was dissolved in isopropanol and delivered by an syringe pump at a flow rate of 0.75 $cm^3 sec^{-1}$ to a nebulizer in order to produce droplets. The droplets were heated for evaporation in the heating column, and the DOS vapor condensed to form submicrometer aerosols. The particles then moved at a flow rate of 3.5 L min^{-1} through a Kr-85 discharger, which lowered their charge to the Boltzmann equilibrium charge level. The neutralizer tube was placed inside an active carbon absorber, which absorbed the isopropanol. The flow rate was increased prior to the particles reaching the test chamber in order to meet test requirements. A mixing fan was placed inside the cone located before the chamber to increase aerosol uniformity. A honeycomb flow straightener was placed between the fan and the chamber to reduce the turbulence. The test chamber was a cylinder (12 inch I.D. x 17 inch long); flow in the test chamber was laminar, and the aerosol concentration was uniform. Pre-filter and post-filter probes were located in the test chamber to sample the aerosols. A magnehelic pressure sensor measured the pressure differential across the test filter. A change in pressure indicated that aerosol particles had built up on the filter. A real-time

aerosol monitor (RAM-1, MIE Inc., Bedford, CT) was connected to the sample probes and measured the mass concentrations before and after the filter. A quartz crystal microbalance (QCM) cascade impactor (Model PC-2, California Measurements Inc., Sierra Madre, CA) determined the aerosol size to be about 0.25μm.

Penetration of Asbestos Fibers in the Filter

Figure 2 shows the experimental apparatus used in the filter penetration studies. Amosite and crocidolite fiber aerosols were generated by a small-scale powder disperser (SSPD, Model 3433, TSI Inc., St. Paul, MN). The SSPD consisted of a rotational disk coated with powder and a suction tube to take up the fibers from the disk and disperse them as an aerosol (Cheng *et al.*, 1995). The aerosol was delivered at a flow rate of 22.5 L min^{-1}. Fine chrysotile fibers were generated by nebulization. The powder was washed and suspended in methanol. The suspension was then nebulized using a Retec nebulizer (InTox Inc., Albuquerque, NM). The aerosol was passed into a ^{85}Kr discharger tube to neutralize the fibers, through a dilutor to maintain proper concentration, and into the test chamber where a small fan and flow straightener distributed the flow evenly. In the case of experiments using charged fibers, the ^{85}Kr discharger was taken out of the delivery line. The test chamber was the same unit used for the DOS penetration experiments described earlier. A fiber air monitor (FAM-1, MIE Inc., Billerica, MA) served as a real-time monitor for fiber concentration flowing through the chamber. An asbestos filter sampler with conductive material (Millipore Corp., Bedford, MA) was used to collect samples in the test chamber for initial fiber concentrations. The filter cartridge was placed in a test assembly. Fibers that penetrated the cartridge were collected in a filter downstream of the test assembly. Twenty-five and 47 mm membrane filters (mixed cellulose acetate and nitrate, Millipore, Bedford, MA) were used in upstream and downstream samplers. The pressure in the test chamber and the pressure drop across the test cartridge were monitored to verify that the desired flow rates were maintained. Each filter cartridge was tested at both flow rates with both charged and neutralized fibers, then treated with the antistatic spray and retested.

Penetration Through Respirator Leaks

Penetration by three asbestos fibers (in charge equilibrium) through leaks in a half-face commercial respirator certified by NIOSH was investigated using crocidolite fibers. The experimental apparatus is shown in Figure 3. The SSPD was used to disperse the crocidolite fibers. The fiber aerosol passed into a ^{85}Kr discharger tube to neutralize the fibers, through a dilutor to maintain proper concentration, and into the test chamber where a small fan and flow straightener distributed the flow evenly before it was delivered to a large test chamber (15 in I.D.). The chamber had a cone-shaped inlet with a fan to mix the incoming air and a honeycomb flow straightener to provide uniform concentration within the test section of the chamber. A half-face respirator with two high-efficiency filter cartridges (AOR57A, American Optical Corp., Southbridge, MA) was mounted on a simulated human face (fiberglass mannequin). This filter cartridge was chosen because it allowed practically no

penetration by either crocidolite fibers or DOS particles. Therefore, the penetration inside the respirator was presumed to result from leaks in the respirator. The face seal leaks were created by placing holes of 1 or 2 mm diameter near the center of the face mask. Constant flow rates of 32 and 85 L min^{-1} were used. FAM-1 served as a real-time monitor of fiber concentration flowing through the chamber. An asbestos filter sampler with conductive material (Millipore Corp., Bedford, MA) was used to collect samples in the test chamber for initial fiber concentrations. All fibers that penetrated the face mask were collected in a filter inside the mannequin. Twenty-five and 47 mm membrane filters (mixed cellulose acetate and nitrate, Millipore, Bedford, MA) were used in upstream and downstream samplers. The pressure in the test chamber and the pressure drop across the test cartridge were monitored to verify that the desired flow rates were maintained.

Fiber Sample Preparation

The generator, chamber, filter, and samplers for fiber experiments were housed in a vented glovebox enclosure. Each filter cartridge was tested at both flow rates with both charged and neutralized fibers, then treated with the antistatic spray and retested. For each experimental condition, duplicate samples were taken. Filter samples were taken to determine aerosol concentration and diameter/length distribution. Filter samples were coated with carbon in a vacuum coating plant. Copper electron microscope (EM) grids were placed on top of the filter substrate attached to the carbon film. The filter was then placed in acetone for 20 minutes to dissolve the filter substrate. The grids were examined and photographed in a Hitachi-7000 Scanning Transmission EM (STEM, Hitachi Ltd., Tokyo Japan) at a magnification of 2000. The photographic negatives were enlarged to a final magnification of 6000. A series of 10-20 photographs was taken to cover a certain area of grid space. These photographs were then placed together. Individual fibers in the viewing area were counted, and the length and diameter for each fiber were measured with an electronic digital caliper (MAX-CAL, Cole-Parmer Instrument, Niles, IL). Only fibers with aspect ratios > 3.0 were considered in the efficiency calculations. Approximately 200 to 600 individual fibers from each montage were measured to derive a diameter/length distribution for the upstream fiber samples. However, in some cases, the downstream samples contained fewer numbers of particles that penetrated the test filter.

Determination of Fiber Concentration

For each sample, the number of fibers in each diameter and length interval was entered into a table. The number concentrations can be calculated from the sum of fiber counts (N) in the viewing area (A), the sampling volume (V), and the total filter area (A_t):

$$C = \frac{NA_t}{AV}. \qquad (1)$$

This formula assumes that fiber collection on a given filter sample was uniformly distributed. Flow

and particle concentration profiles in both the upstream and downstream field samples were calculated to determine the validity of this assumption. Figure 4 shows the schematic diagram of the 47 mm membrane filter sampler used to collect all fibers penetrating the test respirator filter. The flow profile inside the sampler is plotted in Figure 5. Figures 6 and 7 show the velocity and concentration profiles at the collecting surface of filter. The flow rate through the asbestos filter sampler was 1 L min^{-1}, whereas the flow rate for the downstream filter sampler was between 16, 32, 42.5, or 85 L min^{-1}, the same flow rate as through the test respiratory filter. Figures 5 and 6 show the calculated velocity and particle concentration profile at the collecting surface as a function of radial distance. The results suggested that the velocity and concentration profile were nearly uniform across the collecting surface except near the wall, where they decreased to zero. Based on the calculated concentration and velocity profiles, we concluded that Eq. (1) was valid if samples for EM grids were taken in most areas of the sample filters. We decided to take samples from areas close to the center.

Fiber Size Distributions

From the measured length and diameter for each fiber, a diameter/length matrix can be established for each sample taken during the experiment. The distribution can be expressed as a bivariate lognormal distribution if the diameter and length distributions can be shown to follow lognormal distribution (Cheng, 1986). Figures 8 and 9 show examples of the cumulative length and diameter distributions plotted in log-probability scale for amosite fibers from one experiment. The straight line of cumulative distributions in the log-probability scale is indicative of a log-normal distribution. Data for other fibers were similar (data not shown). Therefore, we can express the fiber length/width distribution with a bivariate lognormal distribution as:

$$f(l,\ d) = \frac{1}{2\pi\beta_L\beta_D\,(1-\tau^2)^{0.5}}\ \exp\left[-\frac{A^2+B^2-2\tau AB}{2(1-\tau^2)}\right]$$

$$A = \frac{(\ln d - \mu_D)}{\beta_D}$$

$$B = \frac{(\ln l - \mu_L)}{\beta_L} \qquad (2)$$

$$\tau = \frac{\beta_{LD}}{\beta_L\beta_D}$$

$$\beta_{LD} = \frac{1}{N-1}\sum_{i=1}^{K}\sum_{j=1}^{M}(\ln l - \mu_L)\ (\ln d_j - \mu_D)\ ,$$

where μ_L and μ_D are the the natural logs of the count median length and diameter (CML and CMD), and β_L and β_D are the natural log of the geometric standard deviations (σ_g) for length and diameter.

Determination of Fiber Penetration

From our data, both the overall and size-specific penetrations of a fiber through each test filter can be obtained. The overall penetration is defined as the ratio of the fiber concentration leaving the test filter (C) and the initial concentration (C_o):

$$P_t = \frac{C}{C_o}. \tag{3}$$

The fiber concentrations C and C_o were calculated from upstream and downstream samples.

The size-specific fiber penetration, P(d,l), is defined as penetration by a fiber with diameter, d, and length, l. The experimental design called for fiber counts in specific size intervals (diameter between d and d +Δd, length between l and Δl) for both upstream and downstream samples to be measured. Therefore, experimental observations of penetration for fibers in such size intervals can be calculated as:

$$P(d,l) = \frac{\left(\frac{A_t\ N(d,l)}{AV}\right)_{downstream}}{\left(\frac{A_t\ N(d,l)}{AV}\right)_{upstream}}. \tag{4}$$

This is called the histogram method; however, its accuracy is limited because there are fewer particles in a specific size range, especially for high-efficiency filters, where few particles downstream of the test filter were observed. The accuracy can be improved if all collected particles can be used for the calculation. One such method has been described by Gentry and his coworkers (1987; 1989). His method involves using a weighing factor for each size class. The penetration for each size class is then calculated by summation of particle counts in all size classes. The weighing factor is chosen to approximate 1 for fibers within the given size interval and to approximate 0 when the size is far away from the given size. The problem in using this method is that the results are influenced by the choice of the weighing factor, and there are no rigorous ways to determine the best weighing factor.

Instead of using the weighing factor, a new method is proposed here. From the size and concentration data obtained in upstream and downstream samples, mathematical expressions may be used to describe these size distributions. The penetration, P(d,l) can then be expressed as:

$$P(d,\ l) = \frac{\lim\limits_{\Delta d \to 0,\ \Delta l \to 0} C\ g(d,\ l)\ \Delta d \Delta l}{\lim\limits_{\Delta d \to 0,\ \Delta l \to 0} C_o\ f(d,\ l)\ \Delta d \Delta l} = \frac{C\ g(d,\ l)}{C_o\ f(d,\ l)}\ , \tag{5}$$

where f(d, l) and g(d, l) are the density functions of size distributions for upstream and downstream samples. These distribution functions are obtained using particles of all sizes in a given sample. For asbestos samples used in this study, the bivariate lognormal distribution can be used, and f(d,l) and g(d, l) are substituted with Eq. (2). From the mathematical equation, we can also obtain the total penetration by integration over all particle sizes:

$$P(d,\ l) = \frac{\int_0^\infty \int_0^\infty C\ g(d,\ l)\ dd\ dl}{\int_0^\infty \int_0^\infty C_o\ f(d,\ l)\ dd\ dl} = \frac{C}{C_o}\ . \tag{6}$$

This result is the same as Eq . (1).

Theoretical Model

Penetration of asbestos fibers in respirator filters can also be studied using filtration theories such as the fan model, which is an idealized filter model with well-defined properties (diameter, packing density, fiber arrangement, and flow resistance). However, it is also a good model to describe aerosol filtration in certain filters, such as wire mesh screens (Cheng *et al.*, 1985) and fibrous filters (Kirsch and Fuchs, 1968). Filtration efficiency through the fan model filter has been developed for spherical particles (Kirsch and Fuchs, 1968; Stechkina *et al.*, 1969; Cheng *et al.*, 1990). We have verified the filtration theory for the fan model filter using monodisperse aerosols with wire mesh screens and have demonstrated that the aerosol penetration can be expressed as (Kirsch and Stechkina, 1978; Cheng *et al.*, 1985):

$$P(d, l) = \exp[-(\frac{4\alpha h}{\pi(1-\alpha)d_f})\eta], \quad (7)$$

where α is the solid volume fraction of the fiber, d_f is the screen fiber diameter, and h is the thickness of the filter units. The single fiber efficiency, η, in Eq. (7) summarizes the following mechanical deposition processes, including diffusion, interception, and impaction:

$$\eta = 2.7Pe^{-2/3} + \frac{1}{k_o}R^2 + 1.24\frac{1}{k_o^{1/2}}Pe^{-1/2}R^{2/3} + \frac{1}{4k_o^2}ISt, \quad (8)$$

where k_o is the hydrodynamic factor of the filter, and I is a function of α and R. The parameters representing diffusion, interception, and impaction are: (1) Peclet number ($Pe = d_fU/D$), (2) intercept parameter ($R = d_p/d_f$), and (3) Stokes number ($St = \rho_o d_{ae}^2 UC/18\mu d_f$), respectively, where U is the facial velocity; ρ_o is the unit density; d_p, d_{ae} are the particle diameter and the aerodynamic equivalent diameter, respectively; C is the slip correction factor; D is the diffusivity of the particle; and μ is the viscosity of air.

For a fiber aerosol of diameter, d, and length, l, the aerodynamic equivalent diameter, d_{ae} is defined as (Kasper, 1982):

$$d_{ae} = d_v\sqrt{\frac{\rho C(d_a)}{\kappa\rho_o C(d_{ae})}}, \quad (9)$$

where d_v ($= (1.5d^2l)^{1/3}$) is the volume equivalent diameter of the fiber, ρ_o and ρ are the unit density and particle density, respectively; d_a is the adjusted diameter for fiber (Dahneke, 1973; Cheng, 1991); and C(d) is the slip correction factor with respect to diameter, d. The dynamic shape factor, κ, of the fiber aerosol in random orientation can be expressed as the following function of the aspect ratio (β = l/d) (Kasper *et al.*, 1985; Cheng, 1991):

$$\frac{1}{\kappa} = \frac{1}{3}(\frac{3\ln(2\beta) - 0.5}{\beta^{2/3}} + \frac{3\ln(2\beta) + 0.5}{4\beta^{2/3}}). \quad (10)$$

The diffusion coefficient of the fiber aerosol is defined as (Spurny *et al.*, 1986):

$$D = \frac{kTC(d_a)}{\kappa 3\pi\mu d_v}, \quad (11)$$

where k is the Boltzmann constant, and T is the temperature.

RESULTS AND DISCUSSION

Surface Charge on Filter Cartridges

Negative surface potentials were detected in all four types of filter cartridges. The MSA Type A cartridge and 3M 8710 face masks had higher potentials between 800 and 1800 volts, whereas two other types of cartridges had much lower potentials of around 20 volts. The potential varied between individual cartridges of the same type. Treatment with antistatic fluid removed all surface potentials. Figure 10 shows the effects of conditioning under high temperature and humidity. Our data showed that surface charges were reduced substantially within 2 days, and by the sixth day most surface charges were removed.

Penetration of the DOS Aerosol

The DOS aerosol generated in this study had a mass median aerosol dynamic diameter of 0.30 μm and σ_g of 1.27 based on the QCM impactor measurement. The aerosol collection efficiencies in the filter cartridge and face mask are plotted in Figure 11 and Table 2. The effects of flow rate and filter treatment on the collection efficiency of the low-efficiency face mask and the dust/fume/mist filter were similar. In terms of the differences in percent deposition, charge played an important role in increasing the efficiency of the filter, while flow rate had a very small effect on the efficiency of the filter. The dust/fume/mist filter (MSA Type S) achieved a 95% efficiency at 16 L min^{-1} with an untreated cartridge. The collection efficiency decreased to 94.7% when the cartridge was neutralized. Slightly lower efficiency (94.5%) was observed at 42.5 L min^{-1}, and the efficiency decreased further to 93.9 % when the cartridge was neutralized. The collection efficiency was the lowest for the face mask (3M8710) with 84.6% and 78.2% at 32 and 85 L min^{-1}, respectively. These efficiencies were substantially reduced to 44.0 and 34.9%, respectively, when neutralized cartridges were used. The treatment of the filter cartridge had a more significant effect on the face mask than the dust/fume/mist filter because the face mask had a higher surface charge potential, whereas the other filter had minimum surface potential.

Both high-efficiency filters (AOR57A and MSA type A) have efficiencies > 99.97% efficiency of the test filter and were considerably more efficient than the disposable mask or dust/fume/mist filter. The differences between the discharged and untreated filter cartridges were negligible. The flow rate also had little influence on filter performance.

Our results confirmed that both high-efficiency filters indeed had > 99.97% collection of 0.3

0.3 μm oil droplets, whereas the dust/fume/mist filter performed slightly less than the required 95% efficiency, especially when the cartridge was discharged.

Fiber Size Distribution

Figures 12-14 show photos of amosite, crocidolite, and chrysotile collected in samples taken upstream and downstream of filter tests. The measured size and diameter information for each test was compiled into a matrix such as Tables 3 and 4. Figures 8 and 9 plot cumulative distributions of diameter and length. Both cumulative distributions can be fitted into straight lines in a log-probability scale, an indication that the size distribution of these fibers can be expressed as bivariate distributions. The CMD, CML, σ_{gD}, and σ_{gL} for each sample were calculated and are listed in Tables 5 -7. These tables list information on filter tests using the face mask and the dust/fume/mist filter only. For the other two high-efficiency filters, the filter efficiencies were >99 to 100%, but there were not sufficient fibers in downstream samples to determine this kind of information. The upstream samples were similar to those listed in Tables 5-7.

Amosite fibers had CMDs of about 1.6-1.9 μm and CMLs of 0.8-1.4 μm. The amosite fibers that penetrated the respirator filters were shorter and thinner (CML=0.1-0.16 μm and CML=0.6-1.0 μm). Crocidolite fibers were shorter and thinner than the amosite fibers with CMDs of 0.07-0.12 μm and CMLs of 0.58-0.67 μm. The downstream samples of crocidolite were similar in diameter (CMD= 0.07-0.1 μm) and were shorter than the upstream samples (CMD=0.42-0.58 μm). The chrysotile fibers were very thin and long with CMDs of 0.024-0.043 μm and CMLs of 0.70-1.1 μm). Downstream samples of chrysotile had CMDs of 0.025-0.034 μm and CMLs of 0.43-0.85 μm. Based on the size information, we concluded that the shorter fibers had higher penetration rates through the respirator filters, presumably because interception, which favored longer fibers, is an important fiber collection mechanism in these filters.

Fiber Penetration

Total penetration rates of amosite, crocidolite, and chrysotile through the four types of respirator filters are listed in Tables 8-10. These results showed that both the high-efficiency filter and the filter for the powered respirator had similar performance with essentially 100% efficiency for all three types of asbestos. There were small penetrations (<1%) of the MSA Type A filter in some cases. The effects of flow rate and charge status on the filter and aerosol were not obvious. On the other hand, flow rate, aerosol charge, and treatment of the filter significantly influenced the fiber penetration in the MSA type S filter and face mask. The most significant effects of the electrostatic charge were observed in the face mask (3M 8710), which also had the highest surface potential. The untreated face mask (3M 8710) collected over 96% of the charged amosite, crocidolite, and chrysotile. The efficiency decreased slightly for the discharged fibers (94-97%). The filter performance

deteriorated further (60-90%) when the filter masks were completely neutralized by antistatic spray. The poorest performance was observed at the higher flow rate of 85 L min^{-1} when both the face mask and fiber were discharged. Depositions of 55.0%, 29.4%, and 23.5% were observed using amosite, crocidolite, and chrysotile fibers.

The performance of the dust/fume/mist filter was quite different. There were small electrostatic effects observed at 16 L min^{-1}. A higher efficiency was found for the charged fibers than for fiber aerosols in charge equilibrium. The untreated filter cartridges had a slightly higher efficiency than the treated filter. The lowest efficiency was observed for the treated filter with discharged fibers. However, at 42.5 L min^{-1} for the treated filter/discharged fiber, the performance returned to higher efficiency.

Filtration Model and Size-Specific Penetration

Size-specific penetration of fibers was calculated from Eq. (5) based on measured bivariate distributions from upstream and downstream samples. The results were then presented in 2-dimensional contour plots using SigmaPlot software (Jandel Scientific Software, San Rafael). Figures 15 -17 show examples of penetration of amosite, crocidolite, and chrysotile through the face mask. The contours in these plots represent fiber length and diameter with equal penetration probabilities. Contour plots also showed that fibers within a certain size interval had maximum penetration through the face mask. Under the experimental conditions, the maximum penetrable amosite fibers were those shorter than 0.7 and with diameters between 0.05 to 0.1 μm. For crocidolite, the maximum penetration occurred for fibers of the same size characteristics of the amosite. These indicate that the collection mechanisms for these two fibers in face mask were similar at a given conditions. For chrysotile the maximum penetrable size were in a well defined size ranges of length between 0.2-1.5 μm and diameter between 0.02-0.04 μm.

Theoretical calculations of fiber penetration using the filtration model were also performed. A example of the calculation for using the neutralized amosite experiment in treated face mask at 32 L min^{-1} is shown in Figure 18. Similar penetration contours was obtained. Comparison with experimental observation (Figure 17) suggested that the theoretical model had similar penetration probability. The shape of the contour plots is not exactly the same, but the maximum penetratable size is similar.

Penetration of Fibers Through Leaks in the Face Mask

The penetration of crocidolite fiber through leaks in a dual-cartridge half face mask was measured. ARO57A high-efficiency filter cartridges were used because previous tests showed 100% deposition of crocidolite fiber through this type of filter under the same experimental conditions. Table

11 lists the penetration of crocidolite through 1 and 2 mm holes in the mask at total flow rates of 32 and 85 L min^{-1}. Penetration between 5% and 7% were observed for a 2 mm hole and 1% to 1.5% for a 1 mm hole. The effects of the flow rate were not obvious in this study. Size distributions of crocidolite obtained from upstream and downstream test filter are listed in Table 12. Our results suggested that the size distribution did not change significantly after the fibers penetrated the leak. The high penetration of crocidolite through leaks in the mask indicated that such a seal leak is an important consideration in using a respirator for protection against fiber aerosols.

CONCLUSIONS

Our results provide comprehensive information on the performance of respirator filters in protecting workers from inhaling asbestos fibers. We completed all studies proposed in Specific Aims 1 to 5. Four different filter types, including a high-efficiency filter, a dust/mist filter, a filter for a powered respirator (high-efficiency filter), and a disposable face mask, were tested. Only high-efficiency filters performed consistently on both spherical test aerosols and three types of asbestos fibers. The high-efficiency filters tested were >99% efficient in all cases. Neither the surface charge potential of filter cartridges nor the charge status of fibers appeared to affect filter performance. The performance of low-efficiency filters and masks deteriorated when the charge potential on the filter was removed or fiber aerosols were discharged.

The surface charge measurements of the respirator filters showed that some filters, including those used in disposable respirators, are charged to enhance the collection efficiency. Our data also showed that the surface charges were decreased in a high-temperature, high-humidity environment and disappeared after 1 week. While deposition of spherical particles and fibers in the charged disposable filter was enhanced, the collection efficiency of filter cartridges that did not carry electrostatic charges was not. Similar effects were found for the charge status on fibers. The aerosols in equilibrium charge status were found to have lower efficiency than the charged aerosols. Because many aerosols found in the work environment are aged and in the charge equilibrium, our results imply that these aerosols will not be removed as efficiently.

Shorter fibers had a higher penetration, which indicates that fiber interception is an important deposition mechanism. Experimental penetration data were mapped using contours of equal penetration in a two-dimensional plot. The observed data showed one region of maximum penetration for each condition. The mathematical model provides a similar penetration contour. The maximum penetration occurred at the region of fiber diameter and length where the interception and diffusion deposition are at a minimum. Because of filtration of longer fibers, the biological effects of those fibers that are inhaled may be different from the bulk fiber aerosols. These differences may be related to deposition pattern, deposition efficiency, clearance, and biological activities of inhaled fibers.

Fibers could penetrate the face mask seal, with increased penetration for larger leaks. The fibers that penetrated had similar size distributions as the bulk aerosols. Therefore, for respirators with high-efficiency filters, penetration through face mask leaks can be a serious problems for respiratory protection of workers.

ACKNOWLEDGMENTS

The author are indebted to G.A. Feather, K.D. Rohrbacher, E.E. Martinez, and S.D. Pearson for technical assistance and P.L. Bradley for editing. This research was sponsored by the PHS/CDC under Grant 1 R01- OH02922-01A1 from the National Institute of Occupational Safety and Health through the U. S. Department of Energy under Contract No. DE-AC04-76EV01013.

REFERENCES

Brosseau LM. Ellenbecker MJ, and Evans JS: Collection of silica and asbestos aerosols by respirators at steady and cyclic flow. Am. Ind. Hyg. Assoc. J. 51: 420-426, 1990

Cheng YS, Yeh HC, and Brinsko KL: Use of wire screen as a fan model filter. Aerosol Sci. Technol. 4: 165-174, 1985

Cheng YS: Bivariate lognormal distribution for characterizing asbestos fiber aerosols. Aerosol Sci. Technol. 5: 359-368, 1986

Cheng YS, Yamada Y, and Yeh HC: Diffusion deposition on fibrous filters of intermediate porosity. Aerosol Sci. Technol. 12: 286-299, 1990

Cheng YS: Drag forces of nonspherical aerosol particles. Chem. Eng. Commun. 108: 201-223, 1991

Cheng YS, Powell QH, Smith SM, and Johnson NF : Silicon carbide whiskers: Characterization and aerodynamic behaviors. Am. Ind. Hyg. Assoc. J. 56: 970-978, 1995

Dahneke BD : Slip correction factors for nonspherical bodies. III. The form of general law. J. Aerosol Sci. 4: 163-170, 1973

Davis JMG, Addison J, Bolton RE, Donaldson K, Jones AD, and Smith T: The pathogenicity of long versus short fibre samples of amosite asbestos administered to rats by inhalation and intraperitoneal injection. Br. J. Exp. Pathol. 67: 415-430, 1986

Drew RT, Kuschner M, and Bernstein DM: The chronic effects of exposure of rats to sized glass fibres. Ann. Occup. Hyg. 31: 711-729, 1988

Environmental Protection Agency: 40 CFR 763, Subpart G, 1986 Toxic Substances Control Act: Asbestos

Gentry JW: Determination of size dependent classifier efficiencies from small samples. Staub. 47(5/6): 143-145, 1987

Gentry JW, Spurny KR, and Schörmann J: Collection efficiency of ultrafine asbestos fibers: experimental and theory. Aerosol Sci. Technol. 11: 184-195, 1989

Kasper G.: Dynamics and measurement of smoke. I. Size characterization of nonspherical particles. Aerosol Sci. Technol. 1: 187-199, 1982

Kasper G, Niida T, and Yang M: Measurement of viscous drag on cylinders and chains of spheres with aspect ratio between 2 and 50. J. Aerosol Sci. 16: 535-556, 1985

Kirsch AA and Fuchs AA: Studies on fibrous aerosol filters. III. Diffusional deposition of aerosols in fibrous filters. Ann. Occup. Hyg. 11: 299-304, 1968

Kirsch AA and Stechkina IB: The theory of aerosol filtration with fibrous filters. In: Fundamentals of Aerosol Science (ed. DT Shaw), Wiley, NY, pp. 165-255, 1978

Liu BYH and Lee KW: An aerosol generator of high stability. Am. Ind. Hyg. Assoc. J. 36: 681-685, 1975

National Institute for Occupational Safety and Health: Revision of Tests and Requirements for Certification of Permissibility of Respiratory Protective Devices Used in Mines and Mining. Department of Health and Human Services. 42 CFR, Part 84, 1987

National Institute for Occupational Safety and Health: Respiratory Protective Devices; Test for Permissibility; Fees. Department of Health and Human Services, 30 CFR, Part 2, 1990

Ortiz LW, Soderholm SC, and Valdez SO: Penetration of respirator filters by an asbestos aerosol. Am. Ind. Hyg. Assoc. J. 49: 451-460, 1988

OSHA: Occupational Health and Environmental Controls: Asbestos, Tremolite, Anthophyllite, and Actinolite. 29 CFR 1926, 58, Department of Labor, 1986

Pott F, Stöber W, and Spurny K: Properties of asbestos and other fibrous dusts with regard to their carcinogenicity. In: Aerosols in the Mining and Industrial Work Environments, Ann Arbor Science, Ann Arbor, MI, pp. 585-596, 1983

Smith DM, Ortiz LW, Archuleta RF, and Johnson NF: Long-term health effects in hamster and rats exposed chronically to manmade vitreous fibres. Ann. Occup. Hyg. 31: 731-754, 1987

Spurny K, Weiss G, and Opiela H: On the filtration of fibrous aerosols. Sci. Total Environ. 52: 189-199, 1986

Stanton MF and Wrench C: Mechanism of mesothelioma induction with asbestos and fibrous glass. J. Natl. Cancer Inst. 48: 7, 1972

Stechkina IB, Kirsch AA, and Fuchs NA: Investigation of fibrous filters for aerosol deposition in model filters in the region of maximum particle breakthrough. Colloid J. 31: 97-101, 1969

Stöber W: Dynamic shape factors of nonspherical particles. In: Assessment of Airborne Particles (ed. CW Thomas), Springfield, IL, pp. 249-289, 1973

Walton WH: The nature, hazards and assessment of occupational exposure to airborne asbestos dust: A review. Ann. Occup. Hyg. 25: 148-149, 1982

Weeks TJ and Burns AF: Performance of dust respirators against a fibrous dust. Am. Ind. Hyg. Assoc. J. 31: 290-293, 1970

PUBLISHED PAPER

Cheng YS, Powell QH, Smith SM, and Johnson NF : Silicon carbide whiskers: Characterization and aerodynamic behaviors. Am. Ind. Hyg. Assoc. J. 56: 970-978, 1995

FUTURE PUBLICATIONS

Cheng YS, Holmes TD, Fan BJ, and Yeh HC: Performance of respirator filters for asbestos fibers (in preparation)

Cheng YS, Fan BJ, and Holmes TD: Penetration of asbestos fiber through respirator filter as a function of fiber dimensions (in preparation)

Cheng YS, Fan BJ, and Holmes TD: Penetration of asbestos fiber through respirator seal leaks (in preparation)

APPENDIX
FIGURES AND TABLES

Figure 1

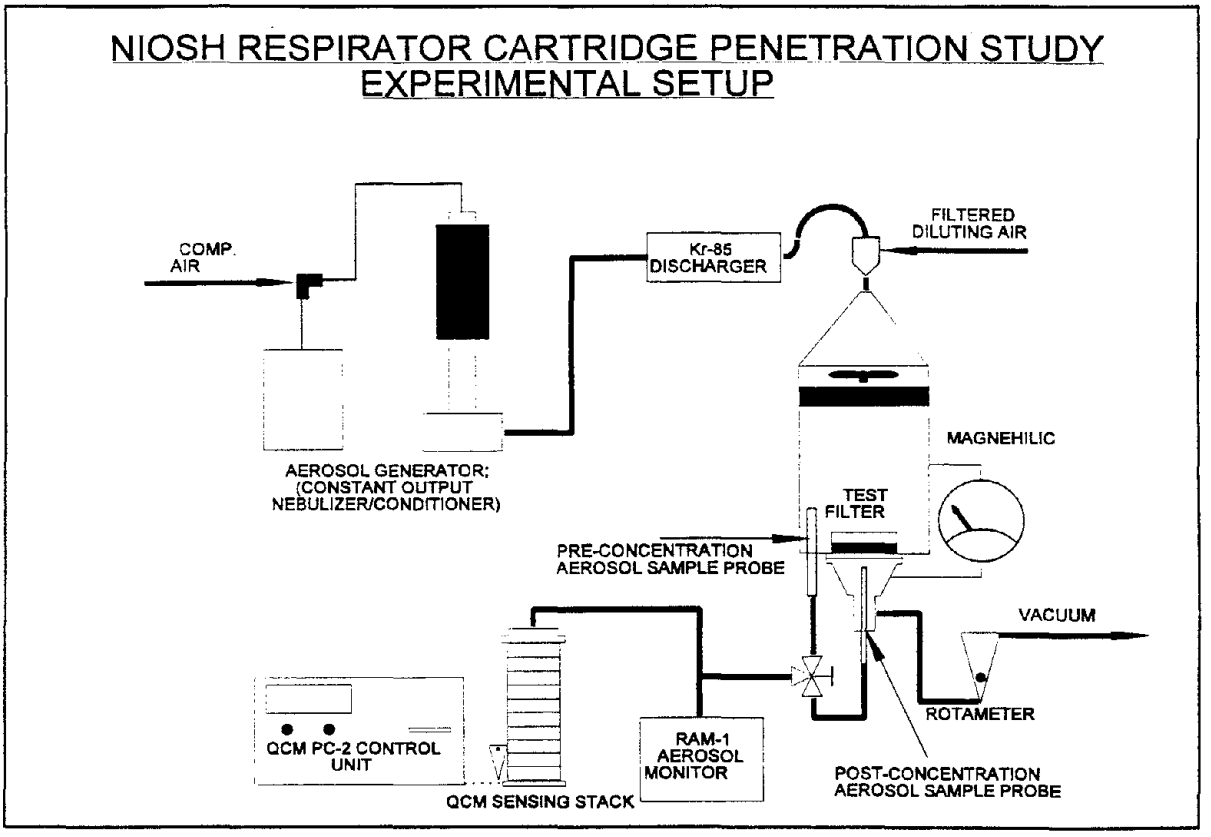

Figure 2

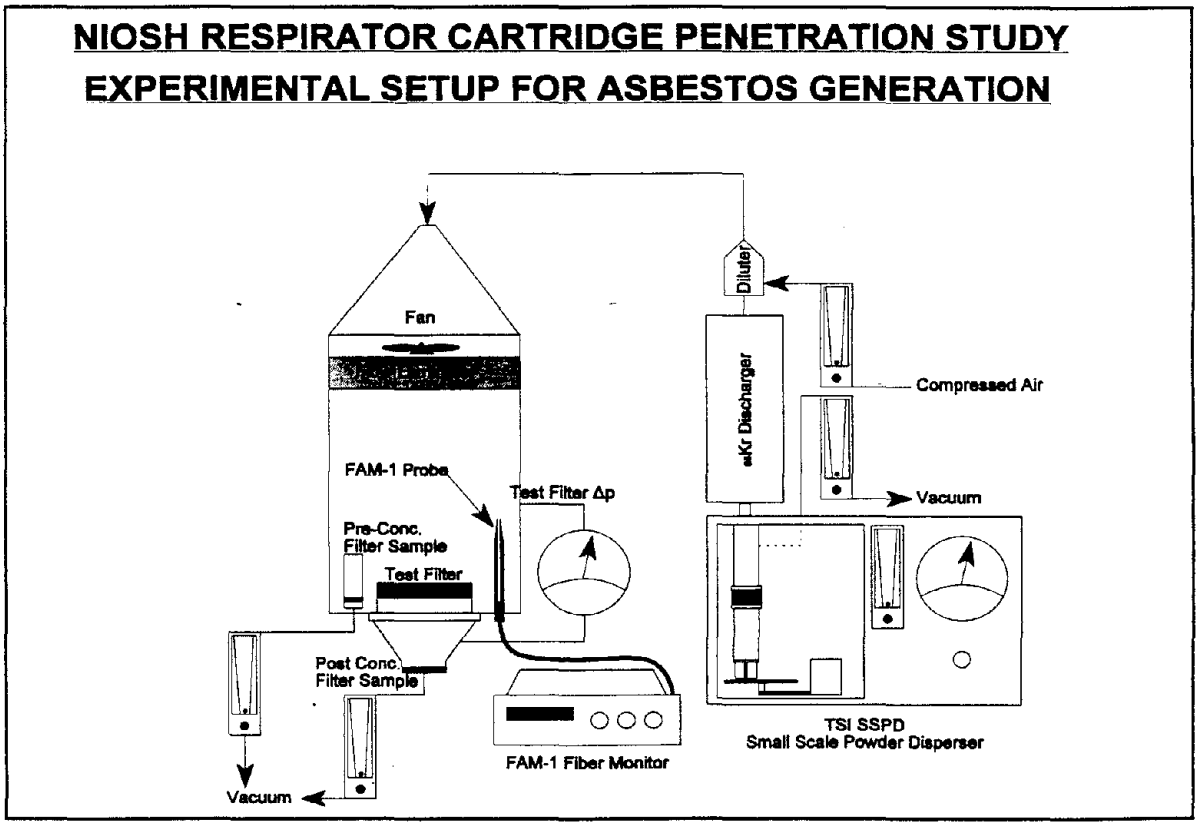

Figure 3

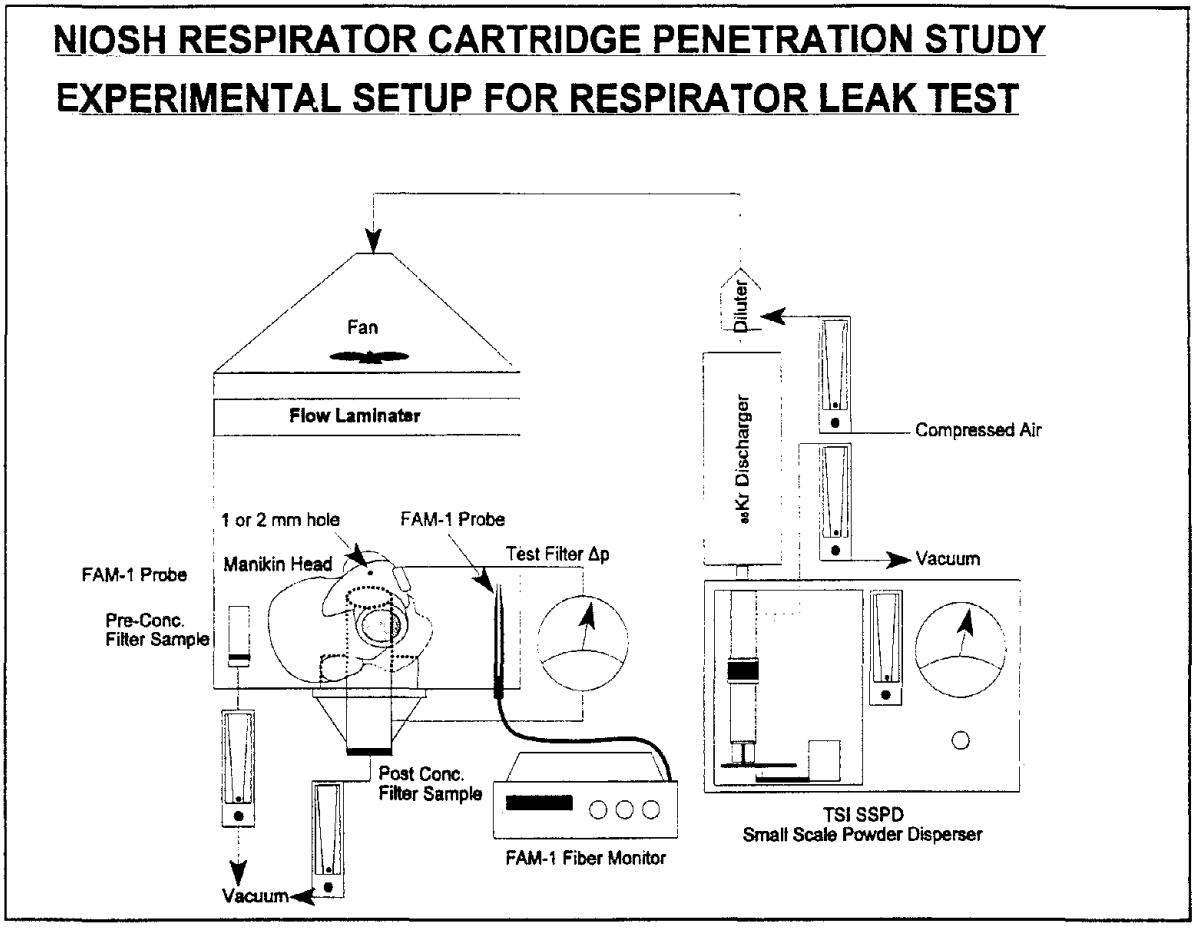
NIOSH RESPIRATOR CARTRIDGE PENETRATION STUDY
EXPERIMENTAL SETUP FOR RESPIRATOR LEAK TEST
Fan
Flow Laminater
Diluter
85Kr Discharger
Compressed Air
Vacuum
1 or 2 mm hole
FAM-1 Probe
Test Filter Δp
Manikin Head
FAM-1 Probe
Pre-Conc. Filter Sample
Post Conc. Filter Sample
FAM-1 Fiber Monitor
Vacuum
TSI SSPD
Small Scale Powder Disperser

Figure 4

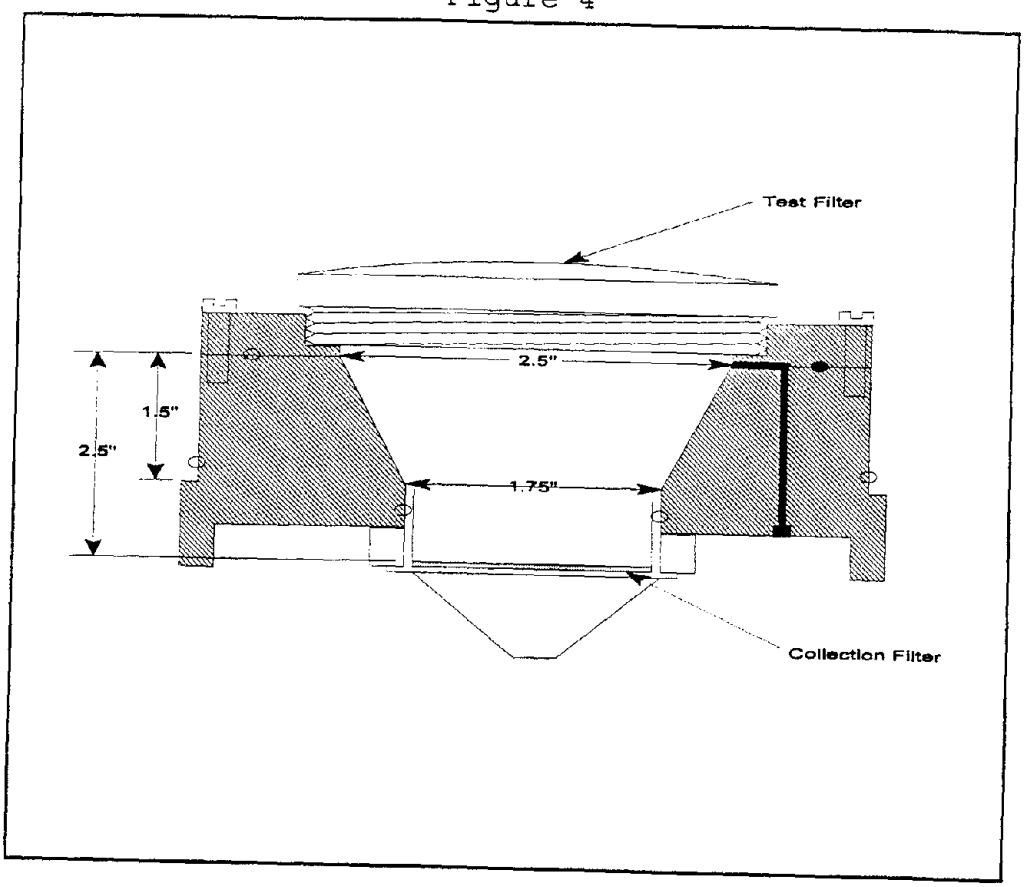

Figure 5

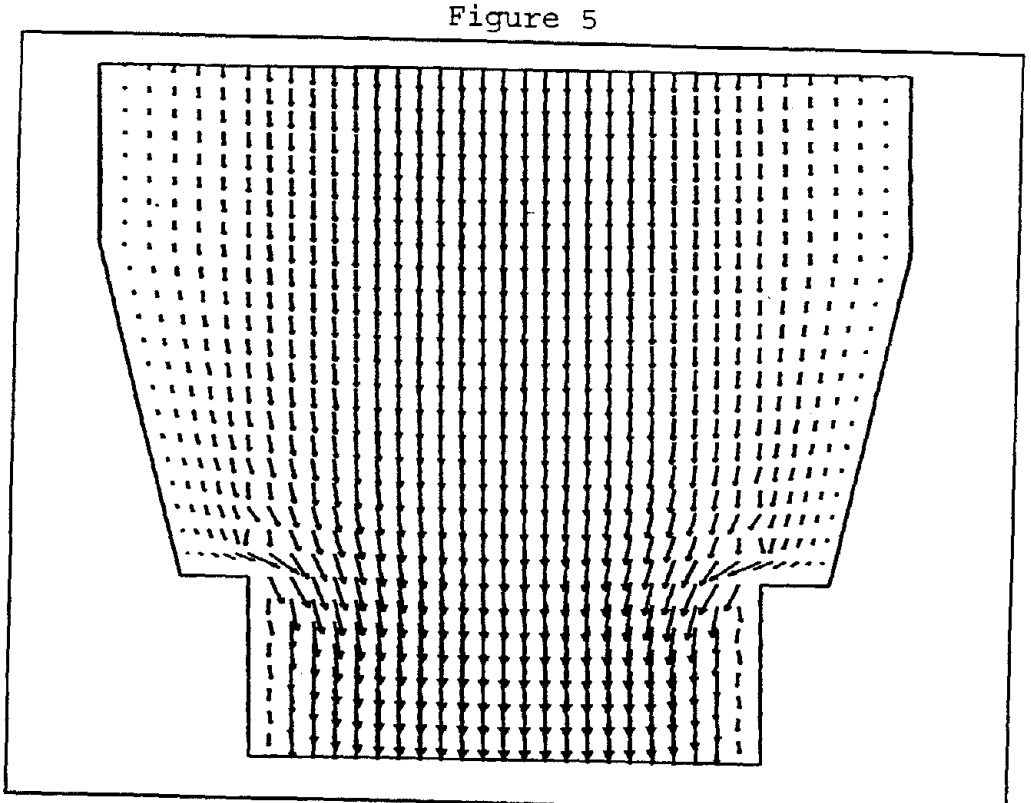

Figure 6

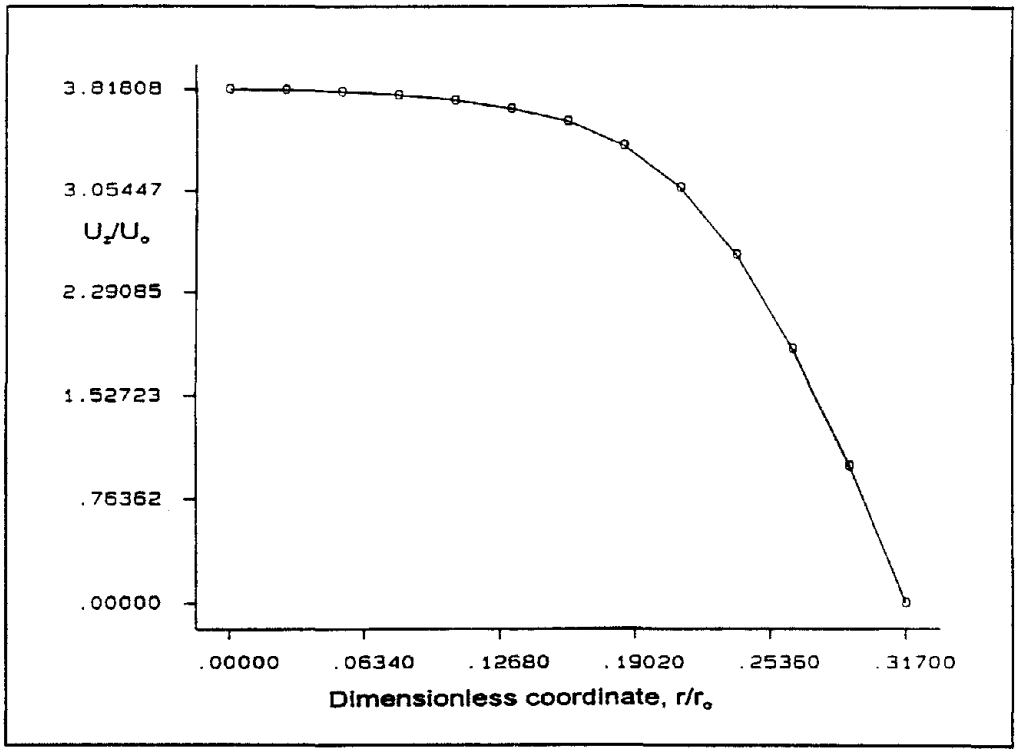

Figure 7

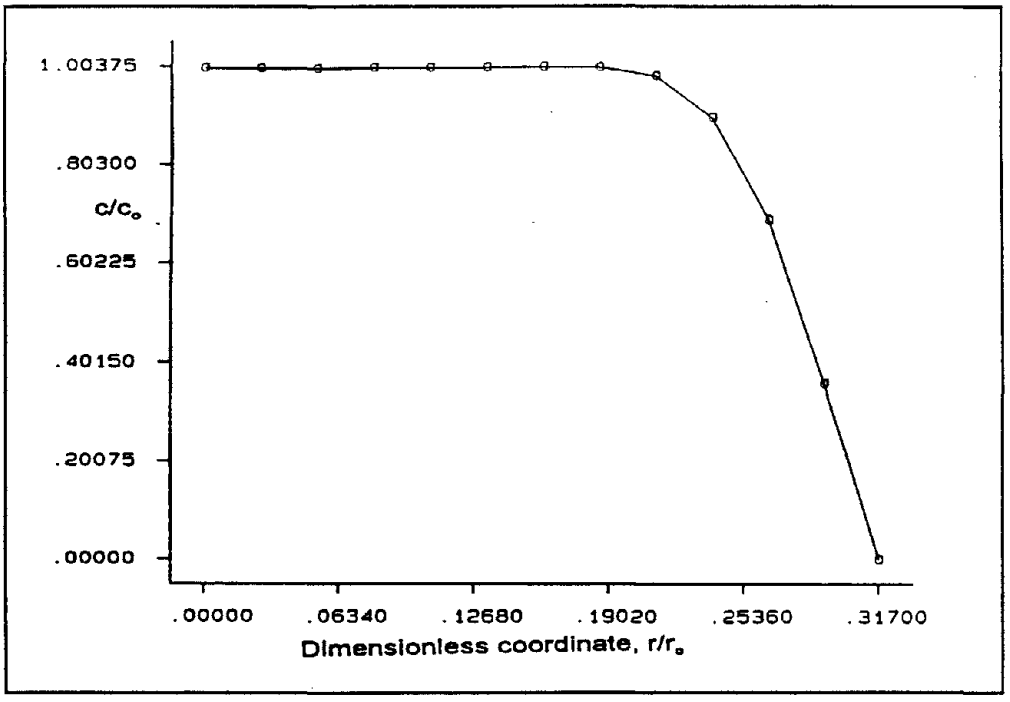

Figures 8 and 9

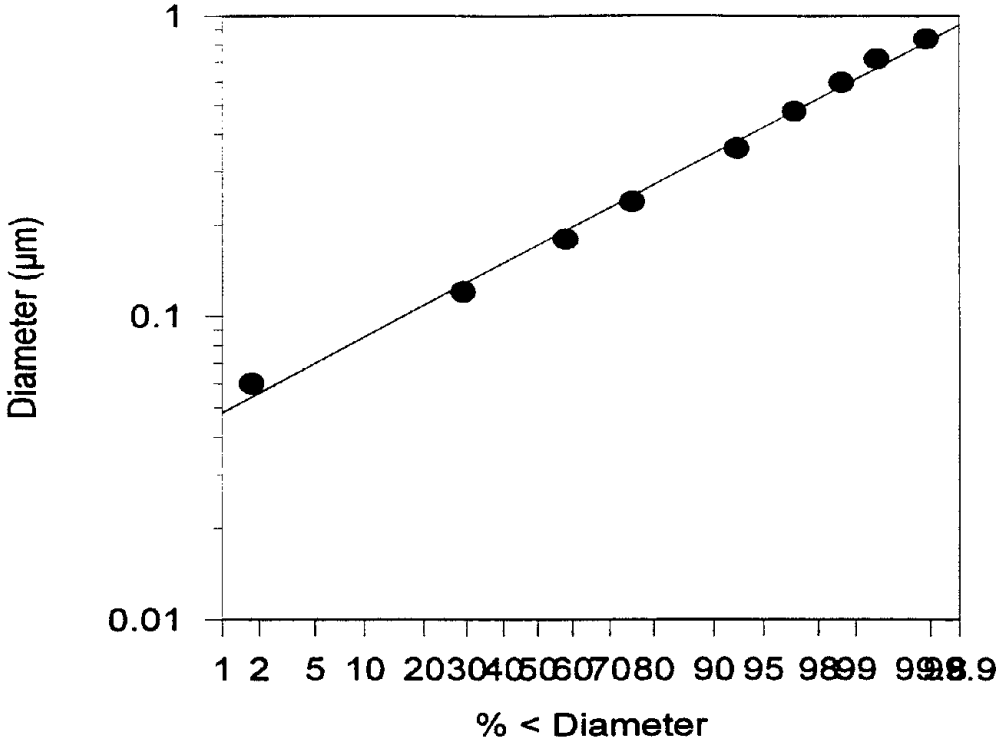

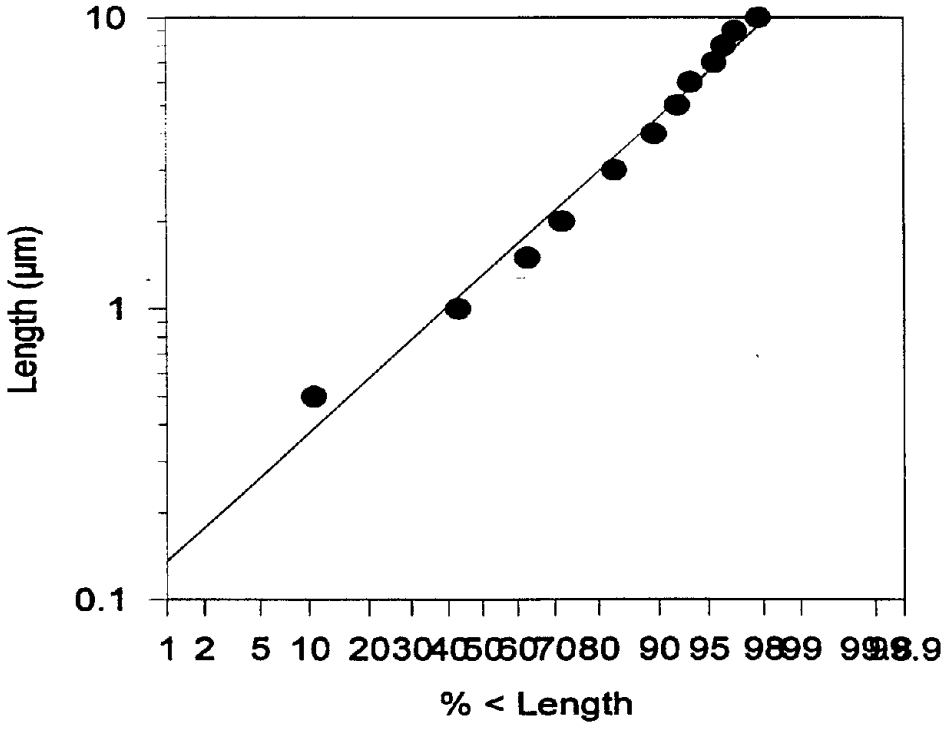

Figure 10

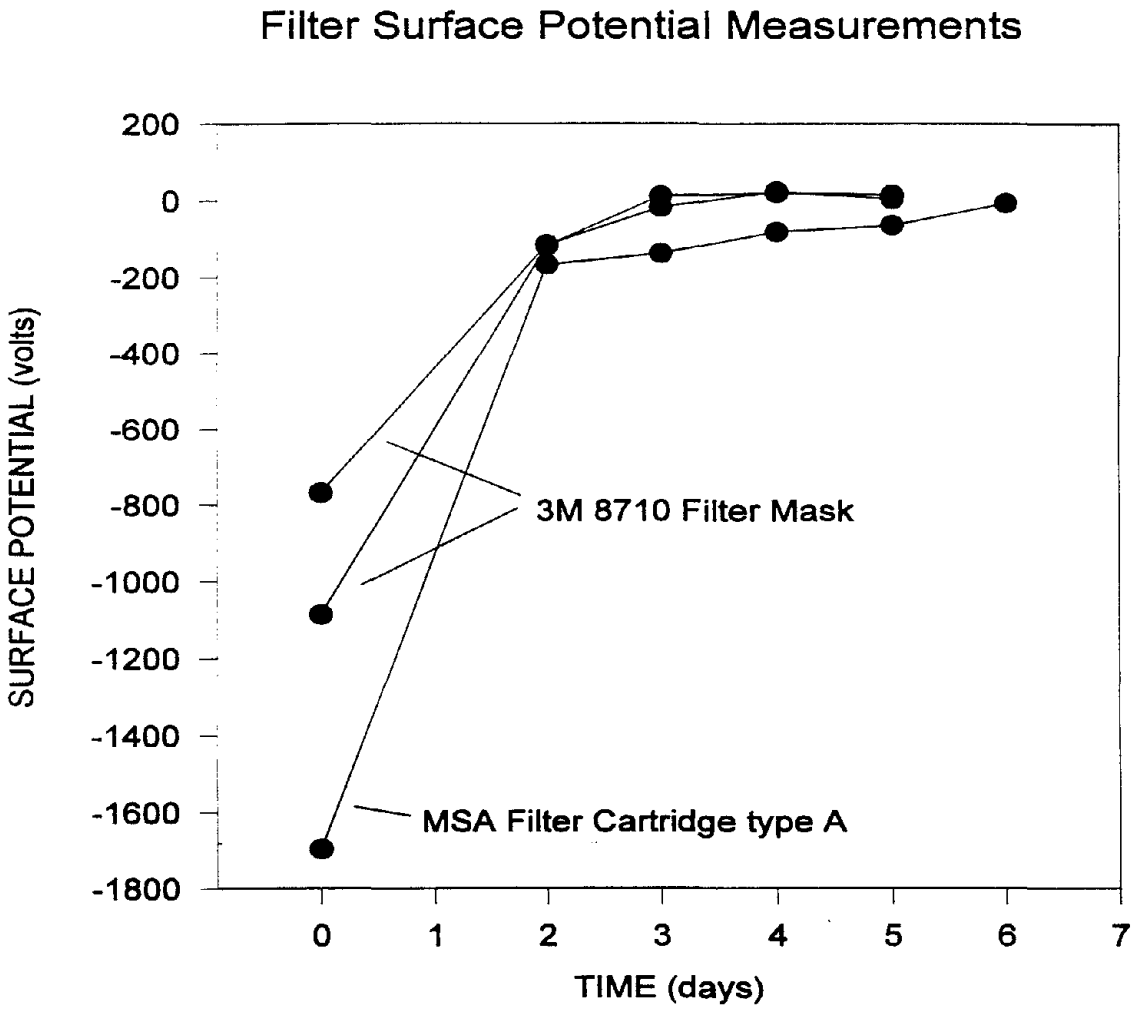
Filter Surface Potential Measurements
SURFACE POTENTIAL (volts)
200
0
-200
-400
-600
-800
-1000
-1200
-1400
-1600
-1800
0
1
2
3
4
5
6
7
TIME (days)
3M 8710 Filter Mask
MSA Filter Cartridge type A

Figure 11

Filter Efficiencies for Neutral 0.3 µm DOS Aerosols

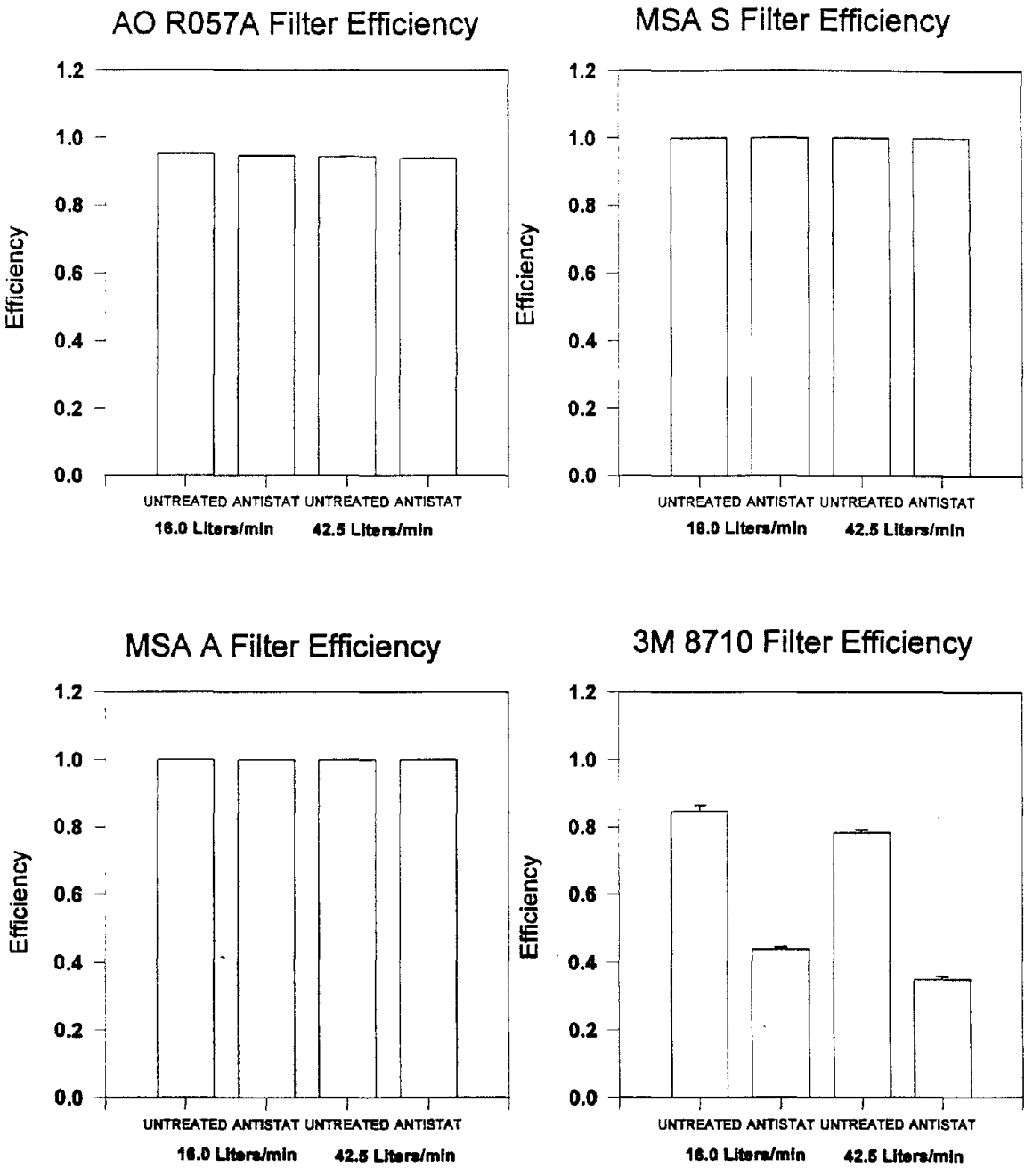

Figure 12(A) and (B)

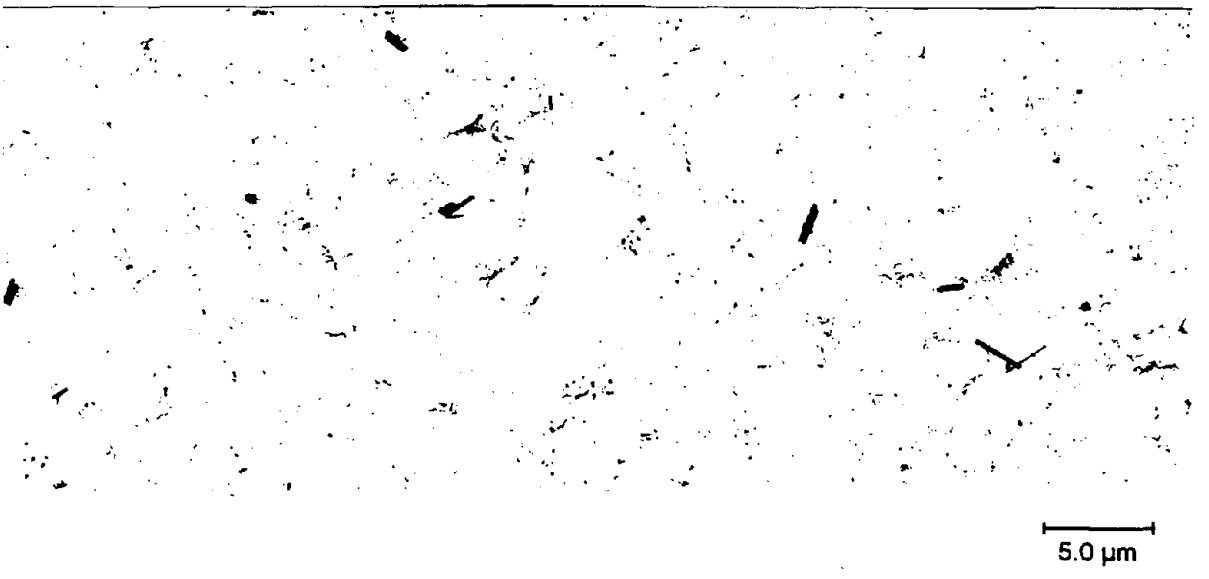

Figure 13 (A) and (B)

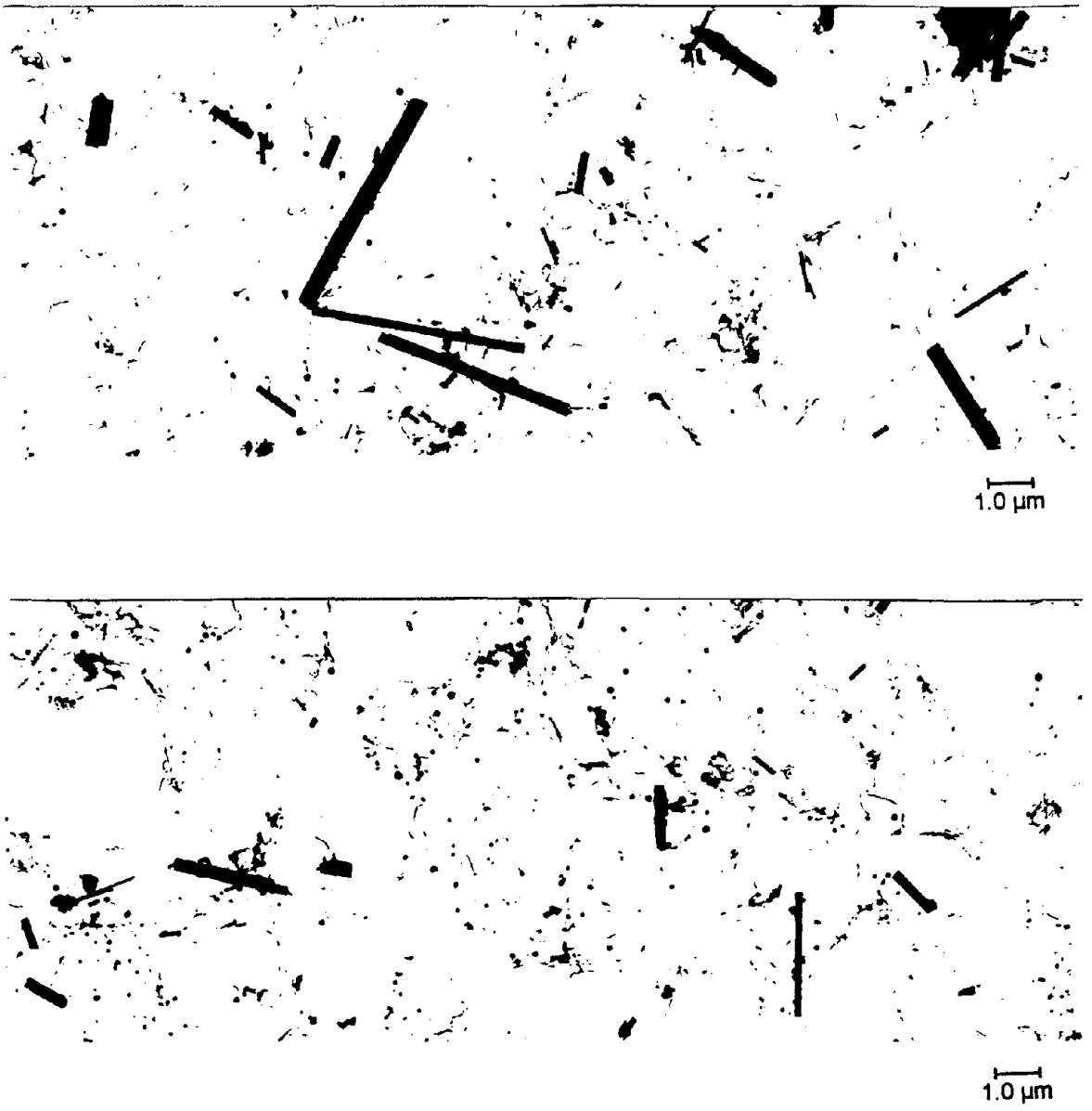

Figure 14 (A) and (B)

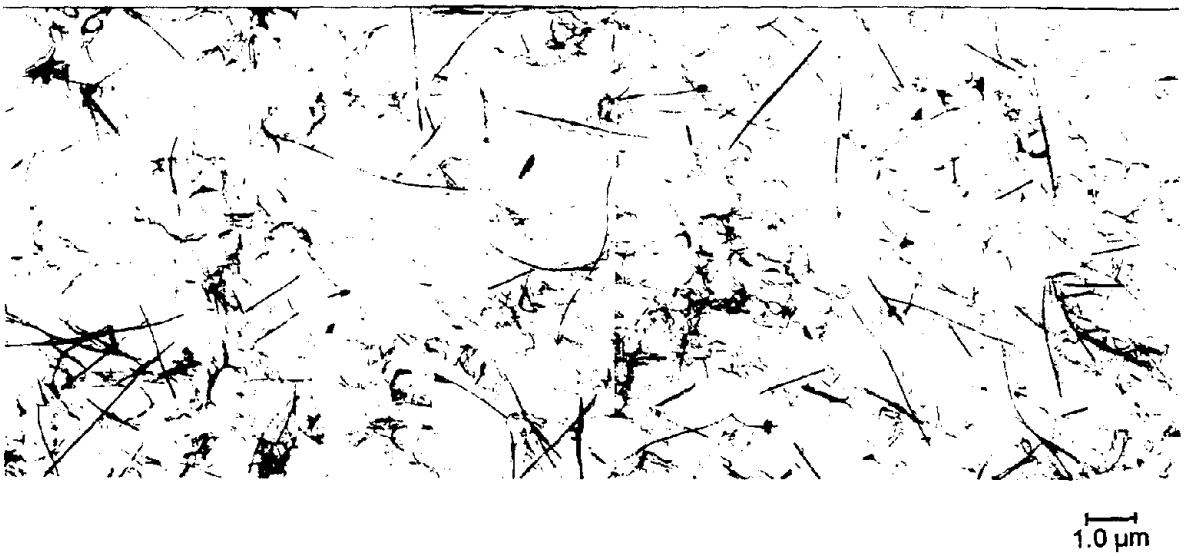

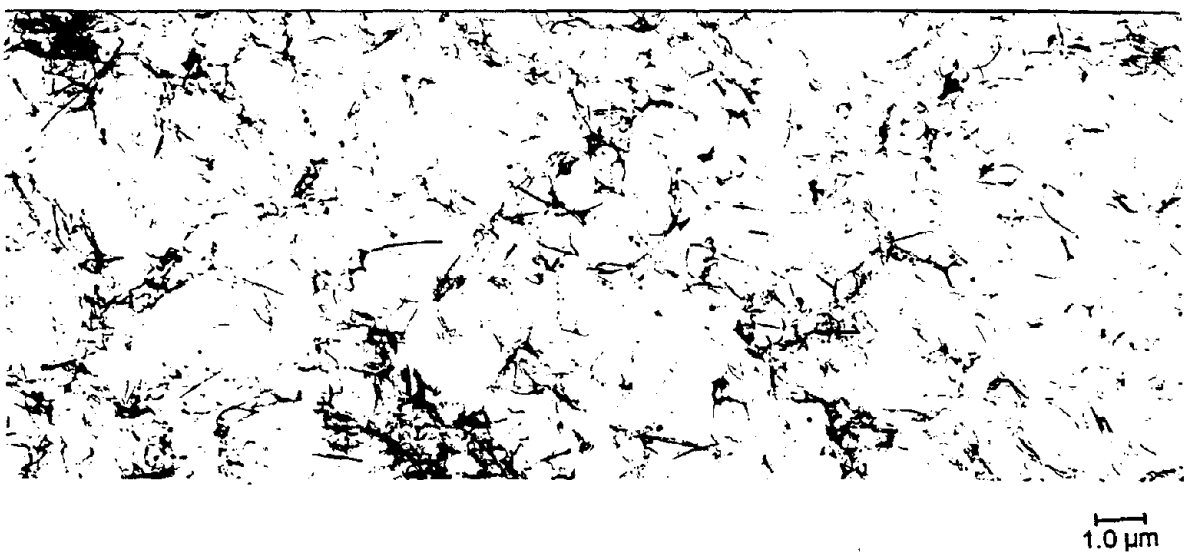

Figure 15

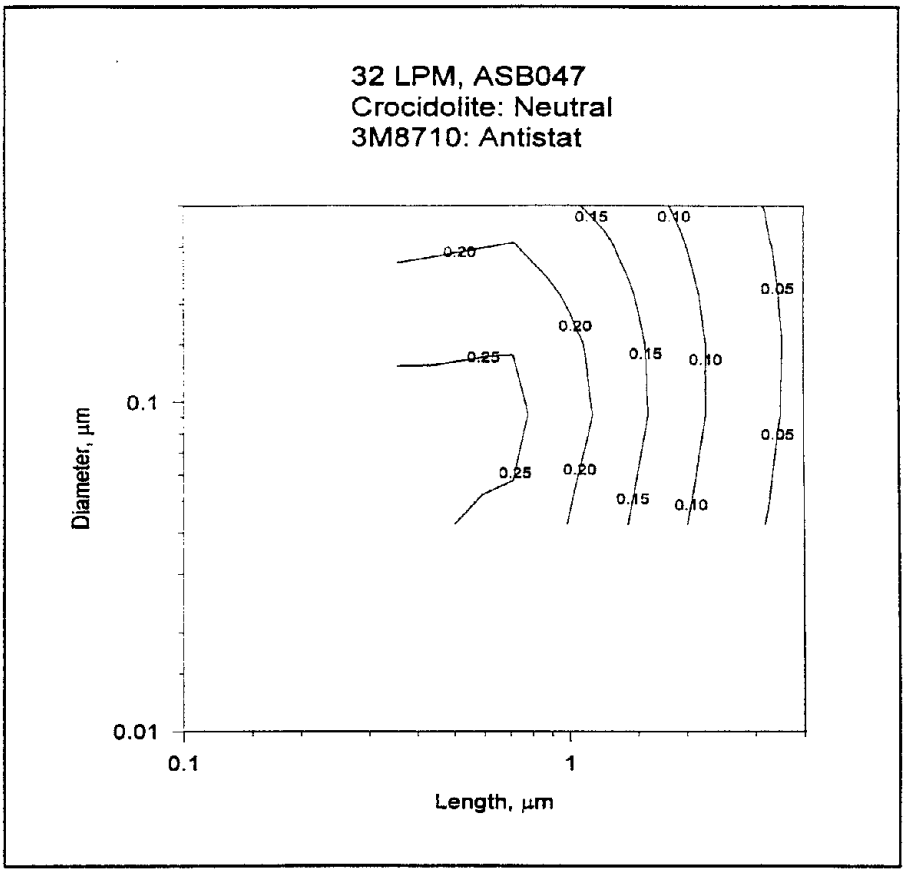

Figure 16

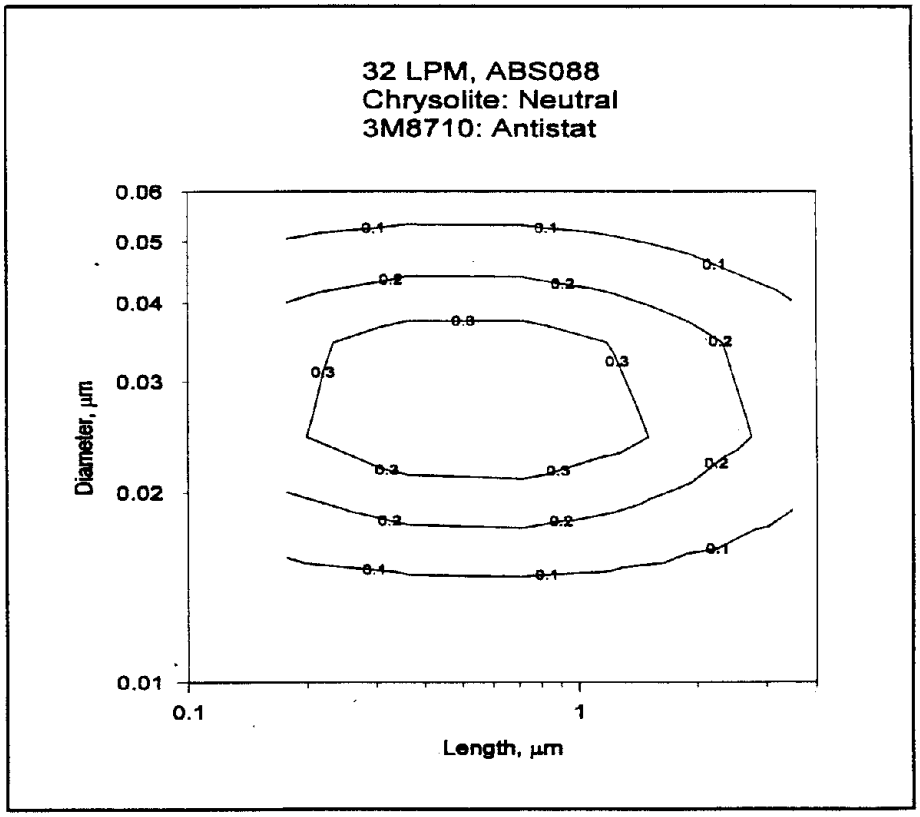

Figure 17

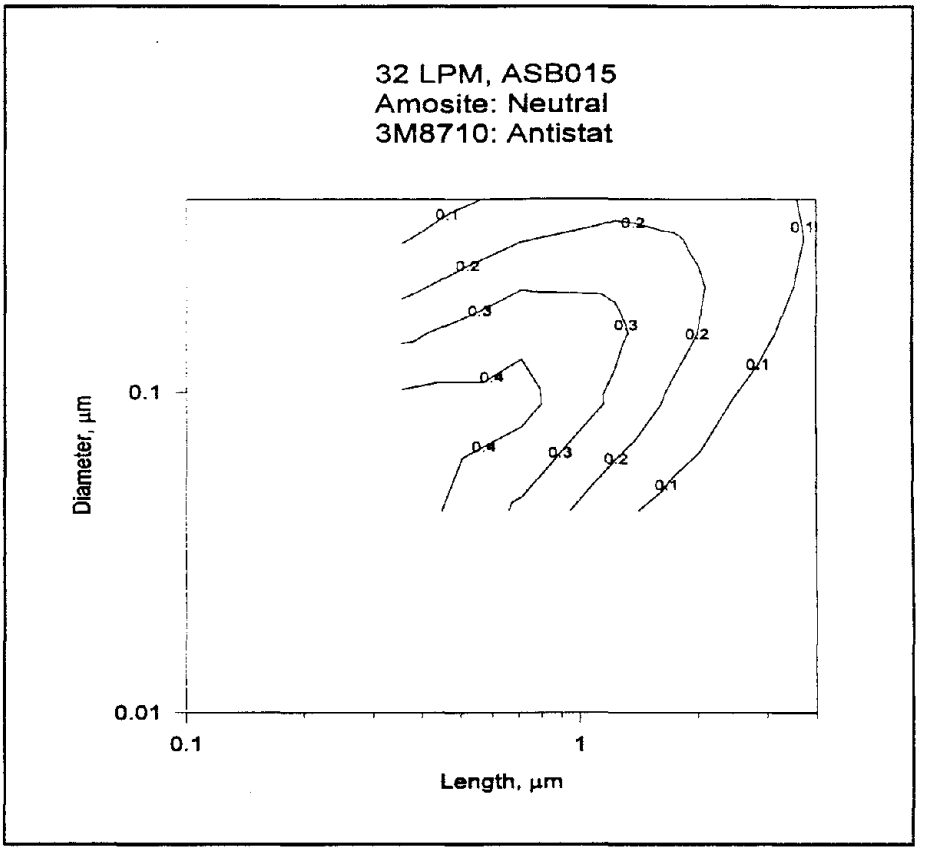

Figure 18

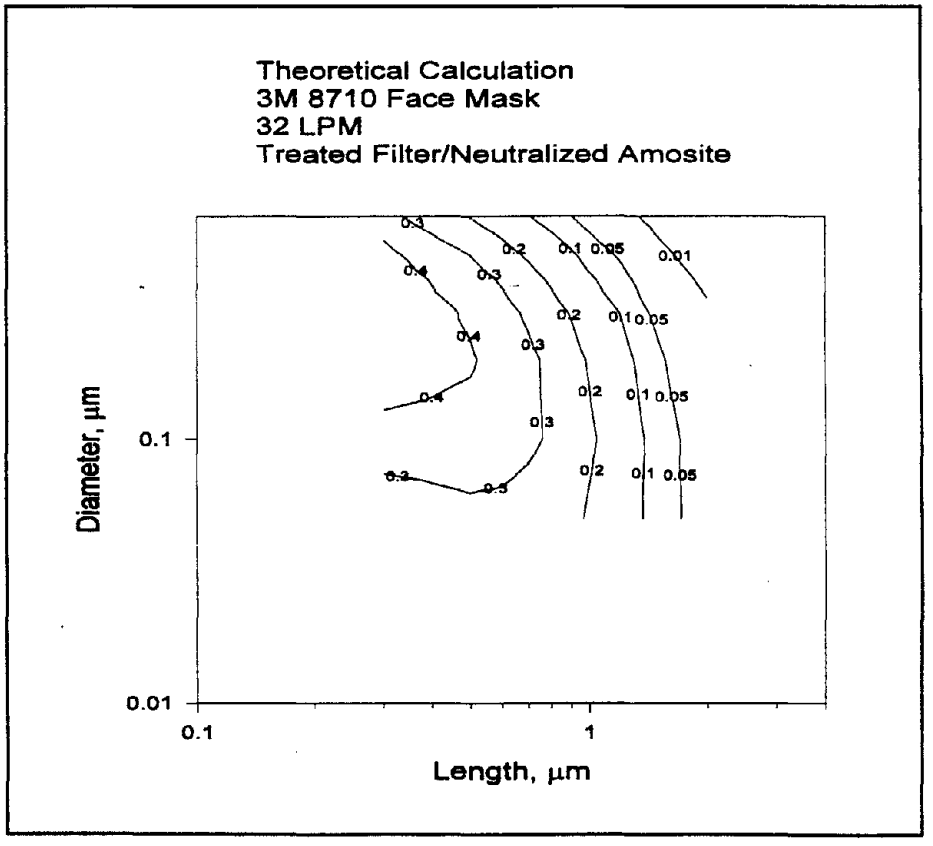

Table 1
Physical Properties of Respirator Filter

Filter	Filter Type	Filter Thickness (cm)	Filter Area (cm^2)	Solid Volume Fraction	Fiber Diameter (μm)	
					Mean	SD
3M 8710 (front layer)	disposable mask	0.0283	177	0.165	25.8	16.3
3M 8710 (middle layer)	disposable mask	0.0573	177	0.114	3.89	0.81
3M 8710 (back layer)	disposable mask	0.100	177	0.116	25.87	5.87
MSA Type S	dust/mist	0.210	353	0.044	2.12	4.53
MSA Type A	power respirator	0.0338	1194	0.056	0.51	0.52
AOR 57A	high efficiency	0.0445	586	0.064	0.30	0.22

Table 2
DOS Aerosol Deposition in the Respirator Filter

Filter Type	Filter Treatment	Flow Rate (L min^{-1})	Aerosol Penetration (%)	
			Mean	SD
3M 8710	untreated	32	84.63	0.0168
3M 8710	neutralized	32	43.96	0.0060
3M 8710	untreated	85	78.17	0.92
3M 8710	neutralized	85	34.93	0.89
MSA Type S	untreated	16	95.21	0.02
MSA Type S	neutralized	16	94.68	0.05
MSA Type S	untreated	42.5	94.45	0.08
MSA Type S	neutralized	42.5	93.92	0.11
MSA Type A	untreated	16	99.99	0.01
MSA Type A	neutralized	16	99.99	0.01
MSA Type A	untreated	42.5	99.99	0.01
MSA Type A	neutralized	42.5	99.99	0.01
AOR 57A	untreated	32	100	0
AOR 57A	neutralized	32	100	0
AOR 57A	untreated	85	100	0
AOR 57A	neutralized	85	100	0

Table 3 Amosite Fiber Distribution in Face Mask Test (Untreated Filter/Charged Fiber) at 16 L min^{-1} Flow
Upstream Sample

Fiber Diameter (μm)

Fiber Length (μm)	0-0.069	0.07-0.129	0.13-0.189	0.19-0.249	0.25-0.369	0.37-0.489	0.49-0.609	0.61-0.729	0.73-0.849	0.85-0.96
0-0.5	2	39	8							
0.51-1.0	3	50	59	27	10					
1.01-1.5	2	14	25	20	28	3				
1.51-2.0	0	7	12	9	9	3	2			
2.01-3.0	1	7	11	10	15	4	2	1	1	
3.01-4.0		3	6	6	4	6	2	1	1	
4.01-5.0			3	3	5	1	1			
5.01-6.0		2	2	1	1					
6.01-7.0			2	3	3		1			
7.01-8.0			1		2					
8.01-9.0			1			1				1
9.01-10		2	2		1					
10+		2	2	1	2	2		1		

Total number = 462

Table 4 Amosite Fiber Distribution in Face Mask Test (Untreated Filter/Charged Fiber) at 16 L min^{-1} Flow Downstream Sample

Fiber Diameter (μm)

Fiber Length (μm)	0-0.069	0.07-0.129	0.13-0.189	0.19-0.249	0.25-0.369	0.37-0.489	0.49-0.609	0.61-0.729	0.73-0.849
0-0.5	6	34	8						
0.51-1.0	5	59	79	29	4				
1.01-1.5	1	11	25	22	30	3			
1.51-2.0	1	9	11	10	13	5	1		
2.01-3.0		6	10	7	10	5	2		1
3.01-4.0		1	2	2	5	3			
4.01-5.0			2	0	3			2	
5.01-6.0			0	0	0				
6.01-7.0			1	0	1				
7.01-8.0				1					
8.01-9.0									
9.01-10									
10+									

Total number = 430

Table 5 Amosite Fiber Size Distribution Before and After Test Filters

Filter Type	Filter Treatment	Fiber Charge Status	Flow Rate (L min^{-1})	Upstream Sample		Downstream Sample		Upstream Sample		Downstream Sample	
				CMD	σ_{gD}	CMD	σ_{gD}	CML	σ_{gL}	CML	σ_{gL}
3M 8710	untreated	charged	32	0.182	1.84	0.143	1.58	1.29	2.28	0.81	1.99
3M 8710	untreated	neutralized	32	0.185	1.69	-	-	1.38	2.34	-	-
3M 8710	neutralized	charged	32	0.185	1.69	0.158	1.69	1.38	2.34	1.02	1.88
3M 8710	neutralized	neutralized	32	0.182	1.84	0.149	1.74	1.29	2.28	0.94	1.97
3M 8710	neutralized	neutralized	85	0.168	1.83	0.129	1.66	1.35	2.68	0.78	1.94
MSA Type S	untreated	charged	16	0.155	1.78	0.151	1.72	0.79	2.32	0.58	1.72
MSA Type S	untreated	neutralized	16	0.167	1.98	0.153	1.61	1.09	2.24	0.62	1.80
MSA Type S	neutralized	charged	16	0.167	1.98	0.138	1.75	1.09	2.24	0.76	1.80
MSA Type S	neutralized	neutralized	16	0.185	1.70	0.147	1.74	1.17	2.24	0.72	1.82
MSA Type S	neutralized	neutralized	42.5	0.175	1.82	0.100	1.83	1.07	2.19	0.61	1.72

Table 6 Crocidolite Fiber Size Distribution Before and After Test Filters

Filter Type	Filter Treatment	Fiber Charge Status	Flow Rate (L min^{-1})	Upstream Sample		Downstream Sample		Upstream Sample		Downstream Sample	
				CMD	σ_{gD}	CMD	σ_{gD}	CML	σ_{gL}	CML	σ_{gL}
3M 8710	untreated	charged	32	0.073	1.72	0.071	2.06	0.584	1.85	0.498	1.58
3M 8710	untreated	neutralized	32	0.119	1.93	0.077	1.64	0.633	1.96	0.516	1.69
3M 8710	neutralized	charged	32	0.077	1.76	0.087	1.73	0.612	2.12	0.559	1.70
3M 8710	neutralized	neutralized	32	0.079	1.80	0.077	1.72	0.607	1.97	0.569	1.77
3M 8710	neutralized	neutralized	85	0.077	1.83	0.074	1.73	0.584	2.05	0.505	1.64
MSA Type S	untreated	charged	16	0.069	1.73	0.073	1.66	0.617	2.14	0.522	1.71
MSA Type S	untreated	neutralized	16	0.075	1.82	0.060	1.56	0.576	1.99	0.416	1.47
MSA Type S	neutralized	charged	16	0.094	1.78	0.086	1.68	0.667	1.90	0.569	1.74
MSA Type S	neutralized	neutralized	16	0.079	1.68	0.101	1.59	0.632	2.08	0.580	1.82
MSA Type S	neutralized	neutralized	42.5	0.080	1.76	0.092	1.53	0.663	2.26	0.514	1.61

48

Table 7 Chrysotile Fiber Size Distribution Before and After Test Filters

Filter Type	Filter Treatment	Fiber Charge Status	Flow Rate (L min^{-1})	Upstream Sample		Downstream Sample		Upstream Sample		Downstream Sample	
				CMD	σ_{gD}	CMD	σ_{gD}	CML	σ_{gL}	CML	σ_{gL}
3M 8710	untreated	charged	32	0.043	1.33	0.031	1.43	1.10	2.50	0.434	2.05
3M 8710	untreated	neutralized	32	0.024	1.45	0.026	1.52	0.792	2.61	0.611	2.31
3M 8710	neutralized	charged	32	0.035	1.20	0.034	1.17	0.991	2.66	0.847	2.22
3M 8710	neutralized	neutralized	32	0.028	1.41	0.029	1.44	0.726	2.79	0.666	2.44
3M 8710	neutralized	neutralized	85	0.033	1.18	0.031	1.43	1.13	2.38	0.681	2.29
MSA Type S	untreated	charged	16	0.032	1.22	0.033	1.16	0.915	2.33	0.671	1.92
MSA Type S	untreated	neutralized	16	0.035	1.19	0.030	1.38	0.733	2.46	0.440	1.93
MSA Type S	neutralized	charged	16	0.027	1.41	0.030	1.41	0.694	2.73	0.622	2.29
MSA Type S	neutralized	neutralized	16	0.027	1.41	0.025	1.42	0.936	2.63	0.542	1.77
MSA Type S	neutralized	neutralized	42.5	0.027	1.50	0.026	1.41	0.687	2.58	0.482	2.14

Table 8
Amosite Fiber Deposition in the Respirator Filter

Filter Type	Filter Treatment	Fiber Aerosol Charge Status	Flow Rate (L min^{-1})	Fiber Deposition (%)	
				Mean	SD
3M 8710	untreated	charged	32	99.82	0.032
3M 8710	untreated	neutralized	32	94.16	0.137
3M 8710	neutralized	charged	32	88.82	NA
3M 8710	neutralized	neutralized	32	79.94	0.81
3M 8710	neutralized	neutralized	85	55.00	12.5
MSA Type S	untreated	charged	16	97.44	NA
MSA Type S	untreated	neutralized	16	91.37	NA
MSA Type S	neutralized	charged	16	94.74	NA
MSA Type S	neutralized	neutralized	16	73.16	NA
MSA Type S	neutralized	neutralized	42.5	97.93	NA
MSA Type A	untreated	charged	32	99.83	NA
MSA Type A	untreated	neutralized	32	99.61	NA
MSA Type A	neutralized	charged	32	100	NA
MSA Type A	neutralized	neutralized	32	99.98	NA
MSA Type A	neutralized	neutralized	85	100	NA
AOR 57A	untreated	charged	16	100	NA
AOR 57A	untreated	neutralized	16	100	NA
AOR 57A	neutralized	charged	16	100	NA
AOR 57A	neutralized	neutralized	16	100	NA
AOR 57A	neutralized	neutralized	42.5	100	NA

Table 9
Crocidolite Fiber Deposition in the Respirator Filter

Filter Type	Filter Treatment	Fiber Aerosol Charge Status	Flow Rate (L min^{-1})	Fiber Deposition (%)
3M 8710	untreated	charged	32	96.75
3M 8710	untreated	neutralized	32	95.85
3M 8710	neutralized	charged	32	91.64
3M 8710	neutralized	neutralized	32	74.08
3M 8710	neutralized	neutralized	85	29.39
MSA Type S	untreated	charged	16	96.36
MSA Type S	untreated	neutralized	16	92.57
MSA Type S	neutralized	charged	16	96.96
MSA Type S	neutralized	neutralized	16	88.34
MSA Type S	neutralized	neutralized	42.5	96.92
MSA Type A	untreated	charged	32	100
MSA Type A	untreated	neutralized	32	98.93
MSA Type A	neutralized	charged	32	100
MSA Type A	neutralized	neutralized	32	100
MSA Type A	neutralized	neutralized	85	100
AOR 57A	untreated	charged	16	99.17
AOR 57A	untreated	neutralized	16	100
AOR 57A	neutralized	charged	16	100
AOR 57A	neutralized	neutralized	16	100
AOR 57A	neutralized	neutralized	42.5	100

Table 10
Chrysotile Fiber Deposition in the Respirator Filter

Filter Type	Filter Treatment	Fiber Aerosol Charge Status	Flow Rate (L min^{-1})	Fiber Deposition (%)
3M 8710	untreated	charged	32	100
3M 8710	untreated	neutralized	32	97.40
3M 8710	neutralized	charged	32	59
3M 8710	neutralized	neutralized	32	76.81
3M 8710	neutralized	neutralized	85	23.50
MSA Type S	untreated	charged	16	97.12
MSA Type S	untreated	neutralized	16	99.50
MSA Type S	neutralized	charged	16	99.29
MSA Type S	neutralized	neutralized	16	95.20
MSA Type S	neutralized	neutralized	42.5	97.99
MSA Type A	untreated	charged	32	100
MSA Type A	untreated	neutralized	32	100
MSA Type A	neutralized	charged	32	100
MSA Type A	neutralized	neutralized	32	100
MSA Type A	neutralized	neutralized	85	100
AOR 57A	untreated	charged	16	100
AOR 57A	untreated	neutralized	16	100
AOR 57A	neutralized	charged	16	100
AOR 57A	neutralized	neutralized	16	100
AOR 57A	neutralized	neutralized	42.5	100

Table 11
Crocidolite Fiber Penetration through Leaks in the Respirator Mask

Filter Type	Filter Treatment	Fiber Aerosol Charge Status	Hole Size (mm)	Flow Rate (L min^{-1})	Fiber Penetration (%)
AOR 57A	untreated	neutralized	1	32	1.43
AOR 57A	untreated	neutralized	1	85	0.98
AOR 57A	untreated	neutralized	2	32	5.62
AOR 57A	untreated	neutralized	2	85	6.88

Table 12 Crocidolite Fiber Size Distribution Before and After Face Seal Leak

Filter Type	Filter Treatment	Hole Size (mm)	Flow Rate (L min^{-1})	Upstream Sample		Downstream Sample		Upstream Sample		Downstream Sample	
				CMD	σ_{gD}	CMD	σ_{gD}	CML	σ_{gL}	CML	σ_{gL}
AOR 57A	untreated	1	32	0.074	1.70	0.081	1.89	0.614	2.16	0.652	2.02
AOR 57A	untreated	1	85	0.075	1.69	0.067	1.71	0.605	1.98	0.656	2.21
AOR 57A	untreated	2	32	0.074	1.74	0.075	1.74	0.713	2.27	0.683	2.47
AOR 57A	untreated	2	85	0.076	1.74	0.067	1.69	0.649	2.19	0.584	1.69

BIBLIOGRAPHIC INFORMATION

PB97-105209

Report Nos:

Title: Evaluation of Respirator Filters for Asbestos Fibers. Final Performance Report.

Date: 27 Jan 96

Authors: Y. S. Cheng, B. Fan, T. D. Holmes, and H. C. Yeh.

Performing Organization: Lovelace Biomedical and Environmental Research Inst., Albuquerque, NM. Inhalation Toxicology Research Inst.

Sponsoring Organization: *National Inst. for Occupational Safety and Health, Cincinnati, OH.*Department of Energy, Washington, DC.

Contract Nos: DE-AC04-76EV01013, CDC-1-R01-OH02922-01A1

NTIS Field/Group Codes: 57U (Public Health & Industrial Medicine), 68G (Environmental Health & Safety), 94H (Industrial Safety Engineering)

Price: PC A05/MF A01

Availability: Available from the National Technical Information Service, Springfield, VA. 22161

Number of Pages: 56p

Keywords: *Respirators, *Protective equipment, *Occupational safety and health, *Filters, Asbestos Fibers, Fibrous dusts, Airborne particles.

Abstract: The effects of fiber dimensions, flow rate, and charge status of filter cartridges on the penetration of fiber aerosols were examined, using four types of test respirator filters (two for passive respirators, one for a powered respirator, and one disposal respirator). Some filters were charged to enhance the collection efficiency. Only high efficiency filters performed consistently for both spherical test aerosols and the three types of asbestos (1332214) fibers. The performance of these filters did not appear to be changed by the surface charge potential of filter cartridges and charge status of fibers. When the change potential on the filter was removed and/or fiber aerosols discharged, the performance of low efficiency filters and masks deteriorated for aerosols. The surface charges decreased in a high temperature, high humidity environment and disappeared after 1 week. Shorter fibers had higher penetration rates indicating the fiber interception is an important deposition mechanism.

50272-101

REPORT DOCUMENTATION PAGE	1. REPORT NO.	2.	3. Recipient's Accession No.
4. Title and Subtitle Evaluation of Respirator Filters for Asbestos Fibers			5. Report Date 1996/01/27
			6.
7. Author(s) Cheng, Y. S., B. Fan, T. D. Holmes, and H. C. Yeh			8. Performing Organization Rept. No.
9. Performing Organization Name and Address Aerosol Science Group, Inhalation Toxicology Research Institute, Lovelace Biomedical and Environmental Research Institute			10. Project/Task/Work Unit No.
			11. Contract (C) or Grant(G) No. (C) (G) R01-OH-02922
12. Sponsoring Organization Name and Address			13. Type of Report & Period Covered
			14.

15. Supplementary Notes

16. Abstract (Limit: 200 words) The effects of fiber dimensions, flow rate, and charge status of filter cartridges on the penetration of fiber aerosols were examined, using four types of test respirator filters (two for passive respirators, one for a powered respirator, and one disposal respirator). Some filters were charged to enhance the collection efficiency. Only high efficiency filters performed consistently for both spherical test aerosols and the three types of asbestos (1332214) fibers. The performance of these filters did not appear to be changed by the surface charge potential of filter cartridges and charge status of fibers. When the change potential on the filter was removed and/or fiber aerosols discharged, the performance of low efficiency filters and masks deteriorated for aerosols. The surface charges decreased in a high temperature, high humidity environment and disappeared after 1 week. Shorter fibers had higher penetration rates, indicating that fiber interception is an important deposition mechanism. The maximum fiber penetration occurred in the region of fiber diameter and length where the interception diffusion deposition were at a minimum. These fibers could penetrate the face mask seal, with increased penetration for larger leaks. The fibers that penetrated had sizes similar in distribution to those found in bulk aerosols and may be a major concern for respiratory protection.

17. Document Analysis a. Descriptors

b. Identifiers/Open-Ended Terms NIOSH-Publication, NIOSH-Grant, Grant-Number-R01-OH-02922, End-Date-09-29-1995, Respirators, Personal-protective-equipment, Respiratory-equipment, Asbestos-fibers, Fibrous-dusts, Airborne-particles

c. COSATI Field/Group

18. Availability Statement	19. Security Class (This Report)	21. No. of Pages 54
	22. Security Class (This Page)	22. Price